



Forschungszentrum Karlsruhe
Technik und Umwelt

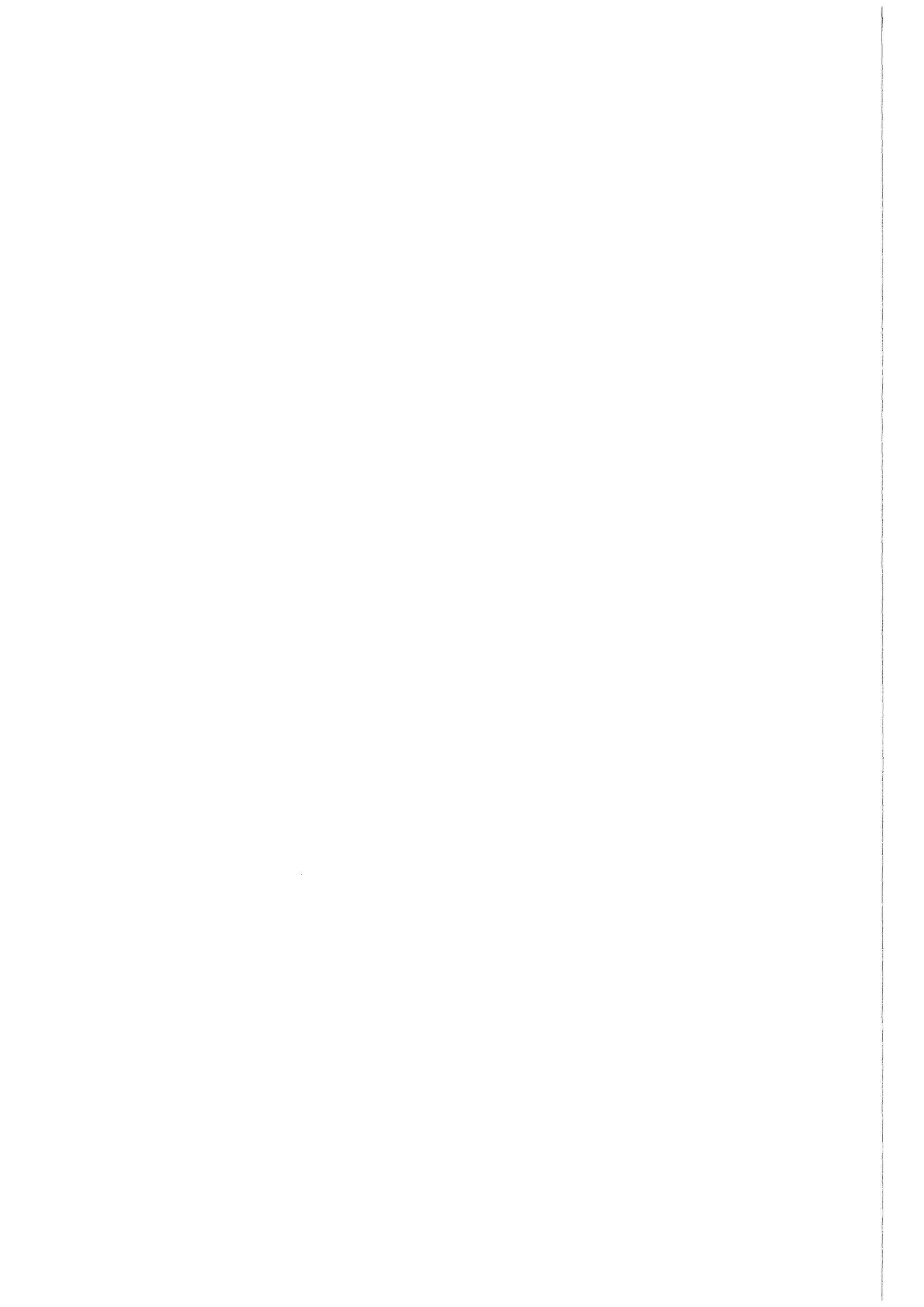
Wissenschaftliche Berichte
FZKA 5978

Thermal Hydraulic Analysis of IFMIF Lithium Target with Incident Deuteron Beam

I. Tiseanu, W. Schütz

Institut für Reaktorsicherheit
Projekt Kernfusion

Oktober 1997



Forschungszentrum Karlsruhe

Technik und Umwelt

Wissenschaftliche Berichte

FZKA 5978

Thermal Hydraulic Analysis of IFMIF Lithium
Target with Incident Deuteron Beam

I. Tiseanu, W. Schütz

Institut für Reaktorsicherheit

Projekt Kernfusion

Forschungszentrum Karlsruhe GmbH, Karlsruhe

1997

Als Manuskript gedruckt
Für diesen Bericht behalten wir uns alle Rechte vor
Forschungszentrum Karlsruhe GmbH
Postfach 3640, 76021 Karlsruhe
Mitglied der Hermann von Helmholtz-Gemeinschaft
Deutscher Forschungszentren (HGF)
ISSN 0947-8620

Abstract

In the proposed International Fusion Materials Irradiation Facility (IFMIF), an intense, high energy neutron flux will be generated by the stripping reaction of deuterons with energy of 30÷40 MeV in a lithium target. The IFMIF target, which should remove up to 10 MW of thermal power, is made of a liquid lithium jet with one free surface (towards the deuteron beam) and a back-wall (towards the test cells). In this design the thermal and hydraulic stability of the lithium jet as well as the evaporation of lithium at the free surface are of major importance. Therefore, the principal objective of this work was to perform a thermal hydraulic analysis of the lithium target jet with incident deuteron beam. The turbulent flow and heat transfer in the target nozzle and in the lithium jet with incident beam have been simulated with the finite element code FIDAP. The profile of the deposited heat due to the stopping of the deuterons has been calculated using models for both electronic and nuclear stopping powers also including the temperature distribution in the target. To our knowledge this is one of the very few studies which includes a consistent simulation of the turbulent flow in both the target nozzle and the jet itself with application to all major target configurations. Although we used a different fluid-flow simulation code and a different lithium properties data set, most of our results for the reference IFMIF target are consistent with those of the IFMIF partner groups. Thus, the surface vaporization proved to be relatively small for beam and jet parameters studied. The free surface at the lower edge of the deuteron beam has been identified as the most critical area for boiling. For relatively low pressures in the vacuum chamber (lower than $p=10^{-3}$ Pa) one can note that the boiling margin at the free surface (for example $\Delta T_b \approx 7$ °C for $p=10^{-4}$ Pa) is the limiting issue of the lithium target design. Boiling margins inside the jet seem to be strongly sensitive on target concepts. In case of the curved back-wall concept, due to the centrifugal force inside the jet the pressure increases quasi-linearly from the reaction chamber pressure until $p \approx 1.3 \cdot 10^4$ Pa near the back-wall such that boiling inside the jet is strongly prevented. For two other concepts, namely the straight back-wall which allows limited internal pressure into the jet, and the free jet target which allows no internal pressure, boiling can be prevented only with the price of a significant increase of average jet velocity and consequently increased lithium inventory. The impact of the amount of vaporized lithium, its deposition and its interaction with the incident deuteron beam need further analysis. In this respect we propose the use of a Monte Carlo Direct Simulation code for modeling of mass and heat transport in the lithium target reaction chamber and in the target-accelerator interface. Finally, we conclude that the results obtained in this study, corroborated with other investigations, have confirmed the physical feasibility of the IFMIF target in the reference curved back-wall configuration.

Thermohydraulische Analyse des IFMIF Lithiumtargets mit einfallendem Deuteronenstrahl

Zusammenfassung

In der vorgeschlagenen „International Fusion Materials Irradiation Facility (IFMIF)“ soll eine intensive hochenergetische Neutronenquelle über die Stripping-Reaktion mit 30 - 40 MeV Deuteronen in einem Lithiumtarget realisiert werden. Das IFMIF-Target, das einen Wärmeeintrag bis zu 10 MW abführen muß, soll aus einem Flüssig-Lithium-Strahl mit einer freien Oberfläche (in Richtung Deuteronenstrahl) und einer Rückwand (in Richtung Testzellen) bestehen. In dieser Auslegung sind die thermische und hydraulische Stabilität des Lithiumstrahls sowie die Verdampfung von Lithium an der freien Oberfläche von besonderer Bedeutung. Hauptgegenstand der vorliegenden Arbeit war die thermohydraulische Analyse des Lithiumtargets mit einfallendem Deuteronenstrahl. Turbulente Strömung und Wärmeübergang in der Targetdüse und im Lithiumstrahl bei einfallendem Deuteronenstrahl wurden simuliert mit Hilfe des Finite-Elemente-Codes FIDAP. Das Wärmeeintragsprofil infolge Deuteronenabbremung wurde mit Modellen für die Stopping Power durch Elektronen- und nukleare Wechselwirkung unter Berücksichtigung der Temperaturverteilung im Target bestimmt. Nach unserer Kenntnis ist dies eine der wenigen Studien, die eine konsistente Simulation der turbulenten Strömung sowohl in der Düse als auch im Strahl enthält und auf alle wichtigen Targetkonfigurationen anwendbar ist. Obwohl ein anderer Simulationscode für den Lithiumstrahl und ein anderer Datensatz für die Lithiumeigenschaften benutzt wurde, sind die meisten unserer Ergebnisse für das IFMIF-Referenztarget konsistent mit denen der IFMIF-Partner. Die Verdampfung von der Oberfläche erwies sich als relativ gering für die untersuchten Parameter des Lithium- und Deuteronenstrahls. Die freie Lithiumoberfläche am unteren Ende des Deuteronenstrahls wurde als der kritischste Bereich für eventuelle Siedevorgänge identifiziert. Für relativ niedrige Druckwerte in der Vakuumkammer (kleiner als $p = 10^{-3}$ Pa) ist festzustellen, daß der Abstand zum Siedepunkt an der freien Oberfläche (z. B. $\Delta T_b \approx 7^\circ\text{C}$ für $p = 10^{-4}$ Pa) der begrenzende Faktor für die Targetauslegung darstellt. Eventuelles Sieden innerhalb des Targets ist stark vom Targetkonzept abhängig. Beim Konzept mit gekrümmter Rückwand kommt es durch die Einwirkung der Zentrifugalkraft innerhalb des Lithiumstrahls zu einem quasilinearen Druckaufbau vom Vakuumkammerdruck bis zu $p = 1,3 \times 10^4$ Pa nahe der Rückwand, wodurch Siedevorgänge innerhalb des Strahles stark unterdrückt werden. Bei den beiden anderen Konzepten, nämlich dem Target mit gerader Rückwand (das einen begrenzten Druckaufbau erlaubt) und dem Freistrahltarget ohne Rückwand (dadurch auch kein innerer Druckaufbau), können Siedevorgänge nur vermieden werden durch eine signifikante Steigerung der Strahlgeschwindigkeit und damit des gesamten Lithiuminventars. Der Einfluß der verdampften Lithiummenge, d. h. ihre Ablagerung und ihre Wechselwirkung mit dem Deuteronenstrahl, bedürfen weiterer Untersuchung. Dazu schlagen wir die Anwendung eines Monte-Carlo-Codes für direkte Simulation vor, um den Masse- und Wärmetransport im Reaktionsraum des Targets und in den Bereichen der Target-Beschleuniger-Wechselwirkung zu modellieren. Schließlich kommen wir, unterstützt durch die Ergebnisse anderer Untersuchungen, zu der Schlußfolgerung, daß unsere Resultate die physikalische Realisierbarkeit des IFMIF-Targets in der Ausführung mit gekrümmter Rückwand bestätigen.

CONTENTS

1. Introduction and background	1
1.1 User requirements.....	2
1.2 IFMIF - Project overview	3
1.3 IFMIF - Target System	4
2. Thermal hydraulic response of lithium target with incident deuteron beam	8
2.1 Modeling assumptions	8
2.2 Modeling tools	10
2.2.1 Computing fluid dynamics models	10
2.2.2 Power deposition model.....	11
2.2.3 Mass and heat transport in the IFMIF reaction chamber	12
3. Results and discussion	14
3.1 Hydraulic analysis of turbulent flow in the target nozzle.....	14
3.2 Thermal hydraulic analysis of the lithium jet with incident deuteron beam.	19
3.3 Boiling margin results	25
3.4 Comparison with other works	31
4. Conclusions	33
References	34
Appendix: Review of lithium physical and thermal properties	36

1. INTRODUCTION AND BACKGROUND

The development of fusion reactors will entail, among others, the elaboration of radiation resistant and low activation materials. These low activation materials must survive exposure to damage from neutrons having an energy spectrum peaked near 14 MeV with annual radiation doses in the range of 20 dpa for iron-based alloys. That explains why the development of materials for fusion reactors is a greater challenge than for any other energy system. The empiricism that the fusion materials development have taken through use of various existing simulation techniques is reaching a saturation, and the risk of uncertainty still remains to be critical for practical applications. It is now a general consensus that in order to test and fully qualify candidate materials up to the expected doses of a fusion power reactor, a high flux source of high energy neutrons, presently not existing, has to be built and operated.

The test facility suitable for such purposes has been explored through a number of international studies and workshops held under the auspices of IEA (International Energy Agency) over the last decade (see Table 1).

Table 1 *The IEA workshops on neutron sources for the fusion materials programme*

San Diego, February 14-17, 1989	<ul style="list-style-type: none">• General definition of requirements of an Intense Neutron Source for Fusion Materials Research• Comparison of different alternatives like stripping, spallation, beam-plasma-reversed field pinch and high density Z-pinch sources
Tokyo, January 14-16, 1991	<ul style="list-style-type: none">• Technical feasibility of accelerator based neutron sources• ESNIT-D-Li, and T-H₂O n-sources
Karlsruhe, September 21-23, 1992	<ul style="list-style-type: none">• Comparison of different sources regarding suitability and feasibility• Comparison of damage parameters in different neutron spectra and for different materials• Conclusion that only D-Li stripping neutron source fulfils presently all selection criteria• Recommendation to start a CDA for an accelerator-based D-Li-neutron source
Karlsruhe September 26-29, 1994	<ul style="list-style-type: none">• Formulate initial requirements and IFMIF-CDA tasks• Established the work breakdown structure for the IFMIF project

At the IEA Workshop in Karlsruhe in 1992 the results of the Neutron Source Working Group were discussed and (taking into account that a selection based only on quantitative criteria such as displacement rate, primary recoil spectrum and important gaseous and solid transmutations was not possible) other criteria like the technical feasibility of different neutron source concepts for given time scale had to be considered. Under the assumption that such a facility should be available not much later than around the year 2000, a neutron source based on D-Li stripping reaction has been selected as the basic concept of the International Fusion Materials Irradiation Facility (IFMIF). The technology of the accelerator-based D-Li neutron source concept was first developed by the Fusion Materials Irradiation Test (FMIT) Project (1978-1984, USA) and later by the Energy Selective Neutron Irradiation Test Facility (ESNIT) Program (1988-92, Japan). Major advances in accelerator technology over the past decade have further added to the credibility of this approach.

A Conceptual Design Activity (CDA) study on IFMIF has been launched under the auspices of the IEA and been performed during 1995-96 by the partners EU, Japan, Russia and USA [Ehrlich 95], [IFMIF-CDA Final Report].

1.1 USER REQUIREMENTS

The design concept of IFMIF is based on input from the materials community on the estimated test volume required to obtain useful irradiation data in a reasonably short operating time. The user requirements as established in the IEA-Workshop in San Diego 1989 are presented in Table 2.

Table 2 *Requirements for an intense neutron source*

-
1. Neutron flux/volume relation: equivalent to 2 MW/m² in 10 l volume (1 MW/m²; 4.5×10¹⁷ n/m²s; E=14 MeV; 3×10⁻⁷ dpa/s for Fe).
 2. Neutron spectrum:
 - should meet FW neutron spectrum as near as possible,
 - quantitative criteria are: primary recoil spectrum PKA, dpa and important gaseous (H, He) and solid transmutations.
 3. Neutron fluence accumulation: DEMO- relevant fluences of 150 dpa in few years.
 4. Neutron flux gradient ≤ 10% based on minimum dimensions of material samples.
 5. Machine availability: 70%.
 6. Time structure: quasi continuous operation.
 7. Good accessibility of irradiation volume for experimentation and instrumentation.
-

$$1 \text{ MWy/m}^2 \approx 10 \text{ dpa for Fe}$$

The stripping reaction means the dissociation of the deuteron in the Coulomb field of the target nucleus. The main characteristics of the D stripping reaction are summarized as follows:

- It gives rise to a narrow forward cone of energetic neutrons whose most probable energy is about 0.4 of the deuteron incident energy. The kinetic energy of the neutron is reduced from the ideal case of 50% of the energy of the incident deuteron by the height of the Coulomb barrier seen by the deuteron and also by the deuteron binding energy ($E_b=2.24$ MeV).

- A thick lithium target is a natural choice for an intense high energy neutron source due to an increased number of atoms within the deuteron range which compensate the decrease with the Z number of the Coulombian cross section.
- One deuteron with an energy of 35 MeV produces 0.05-0.06 neutrons in a thick lithium target.

The user requirements for an intense neutron source could be satisfied only using beam currents of several hundreds of mA. However, it is recognized that the originally specified volume of 10 l for high-flux irradiations with neutron loading of 2 MW/m² and more had to be reduced by one order of magnitude, if a realistic beam-current of 250 mA is assumed for this alternative. On the other hand, the D-Li neutron spectrum produced by deuterons with energy in the range 30-40 MeV is considered to meet essential fusion neutron spectrum requirements, as seen in Table 3, [Ehrlich 97].

Table 3 Gas production and dpa rates for IFMIF compared with fusion reactor values

	appm He / dpa			appm H / dpa		
	Iron	Vanad.	Chrom.	Iron	Vanad.	Chrom.
IFMIF, 30 MeV	7.9	4.3	7.8	44.9	16.6	15.2
IFMIF, 35 MeV	9.1	5.7	10.1	51.9	21.4	16.1
IFMIF, 40 MeV	10.2	7.2	12.4	58.4	25.4	16.7
ITER inboard	11.3	5.5	17.9	44.1	23.0	44.8
DEMO outboard	10.4	4.9	16.1	41.0	20.4	41.3

1.2 IFMIF: PROJECT OVERVIEW

The use of an accelerator to generate neutrons results in a plant with mainly three components:

1. Accelerator Facilities which produce accelerated deuterons,
2. Target Facilities which produce a flowing stream of lithium to convert the accelerated deuterons to neutrons and remove up to 10 MW of thermal power,
3. Test Facilities which expose, package and examine specimens.

Accelerator Facilities

The IFMIF requirement for 250 mA of deuteron beam current delivered to the target will be met by two 125 mA, 40 MeV accelerator modules operating in parallel. Each module comprises a sequence of acceleration and beam transport stages. A cw 155 mA deuteron beam is extracted from the ion source (most probable of ECR type) at 100 keV: A Low Energy Beam Transport (LEBT) guides the deuteron beam from the source to an Radio Frequency Quadrupole (RFQ). The RFQ bunches the beam and accelerates 125 mA to 8 MeV. The 8 MeV beam is injected directly into room temperature, Drift Tube Linac (DTL) of conventional Alvarez type where it is accelerated to 30 to 40 MeV. Finally, the DTL beam is directed to the lithium target by a High Energy Beam Transport (HEBT) section.

The HEBT is required to maintain the beam structure over the long distance, then tailor the beam to provide a flat rectangular beam profile on the flowing lithium target. One should mention that despite relevant success obtained in the last period in accelerator technology there is still need for research especially in development of reliable, high current ion injectors and high energy beam transport and tailoring systems.

Target Facilities

The IFMIF Target Facility shall provide a stable lithium jet in the target assembly for reaction with the deuteron beam to produce high energy neutrons and removal of up to 10 MW of beam power. The lithium loop will contain systems for monitoring and maintaining a high purity of the loop. The total lithium inventory will be 21 m³ (12.6 tons).

The most important element of the Target Facilities is the target assembly itself. Based upon a thorough assessment of various target designs, the modified FMIT-type target with a replaceable backwall has been selected for the baseline design. In this arrangement, the front of the lithium jet is exposed to the accelerator vacuum, and the backwall is slightly curved to enhance both the hydraulic and thermal stability of the jet. It is recognized that the back-wall is a critical component in the target design.

Test Facilities

Test Facilities include two major subsystems, the test assemblies and the Post Irradiation Examination cells. The test assemblies are self-contained packages that position the material specimens in the neutron fluence and provide either NaK or helium cooling to control the specimen temperature. At the end of an exposure campaign, all the specimens are removed and a small percentage of the total are evaluated in the hot cells. The remaining specimens are repacked along with new materials and cycled into the test cell for another campaign. A typical exposure life for different types of specimens will be on the order of ten cycles. An estimate of the test volume and the corresponding displacement rate in a test assembly with iron-based specimens per year of facility operation is as follows: 0.1 l > 50 dpa/fpy, 0.5 l > 20 dpa/fpy and 6.0 l > 1 dpa/fpy.

Neutronics calculations indicate that 40 MeV deuterons provide the maximum high-flux irradiation volume (the neutron yield is 60% higher than for 30 MeV deuterons) and provide a reasonable simulation of the fusion energy gaseous and solid transmutation rates in most metallic materials. Some of the transmutation components in ceramic materials are best simulated with 35 MeV deuterons. The flexibility of choosing deuteron energies between 30 and 40 MeV during irradiation campaigns allows experiments designed to establish the influence of certain transmutation products to be conducted.

1.3 IFMIF TARGET SYSTEM

The target assembly, shown in the Figure 1, consists of a 20 cm interior diameter inlet pipe, a transition component from inlet pipe to a flow straightener, a nozzle, a replaceable backwall, a downstream diffuser with built-in drain baffles and a

vacuum port for connection to the deuteron beam tube. The target assembly is approximately 2.5 m tall and weights about 650 kg. The vertical distance from the highest point of the inlet pipe to the beam centerline is about 1.5 m and ca. 1.0 m from beam centerline to the top of the quench tank. Because of nuclear heating by scattered neutrons, the permanent target structure surrounding the beam footprint will be cooled separately by routing a small lithium stream from the inlet pipe. The test assemblies will be located as close as possible (within 2 mm) to the target backwall to receive maximum neutron fluence.

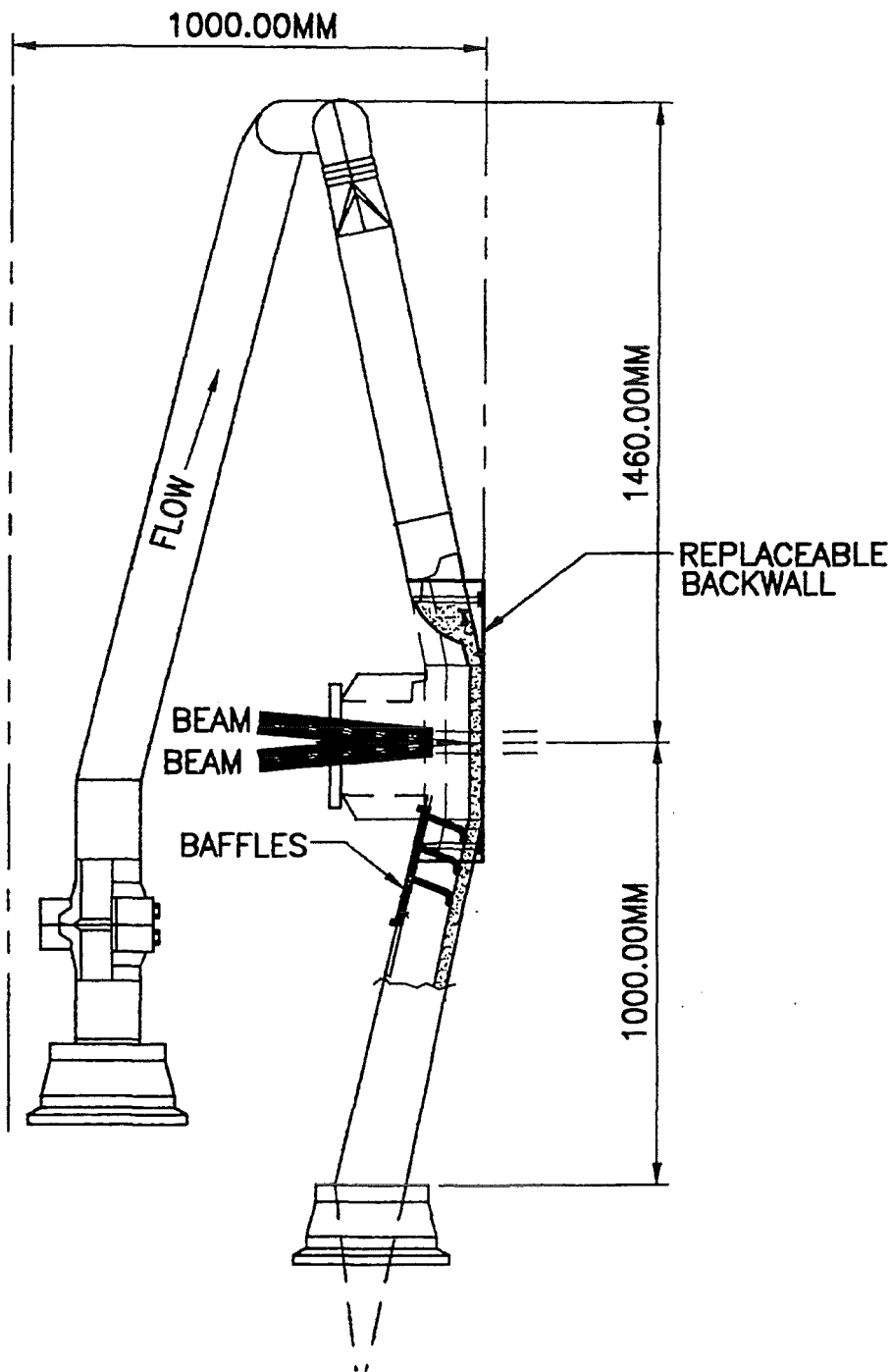


Figure 1. IFMIF target assembly [IFMIF-CDA Final Report]

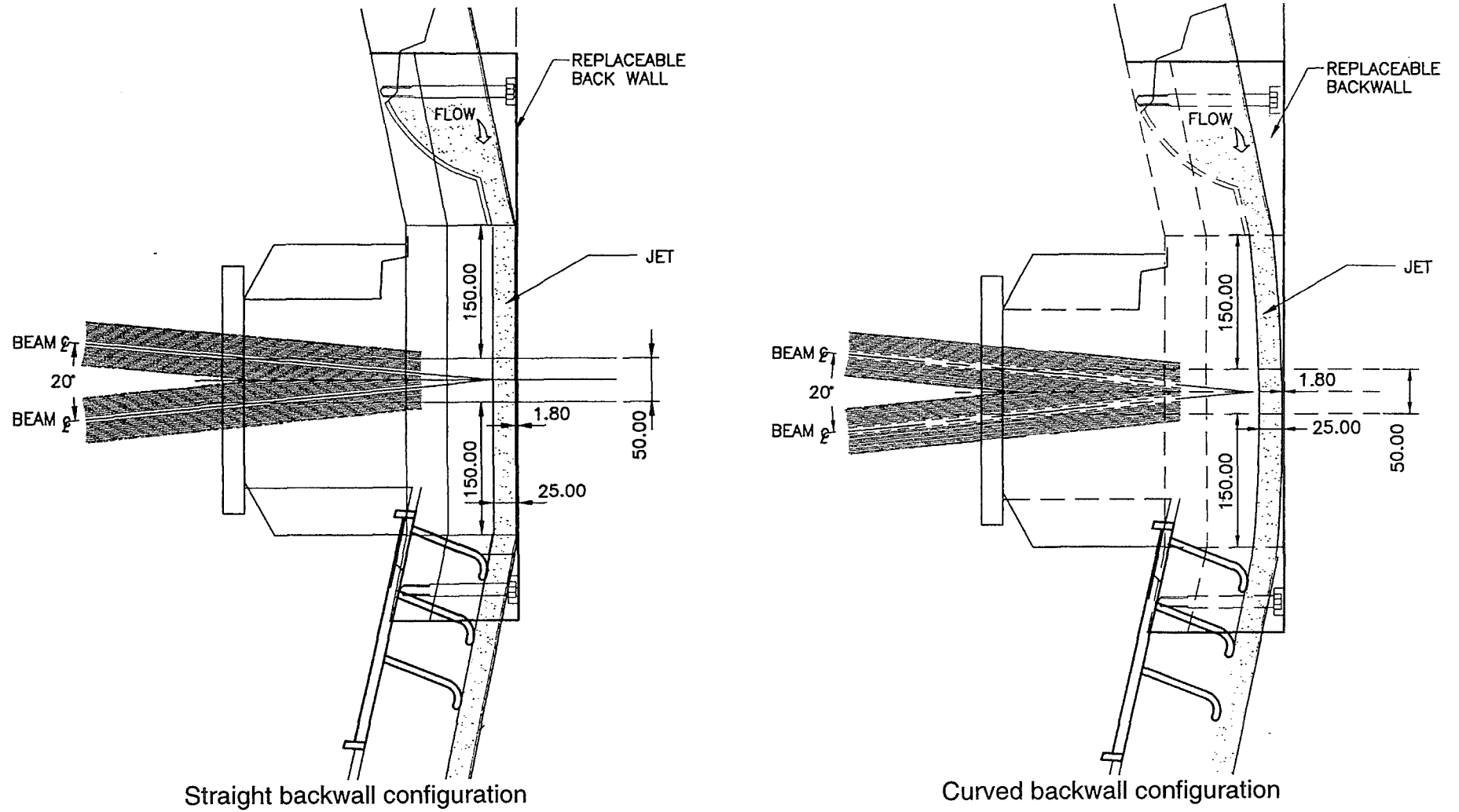


Figure 2. Enlarged view of the beam-on-target region [IFMIF-CDA Final Report]

The wall surface towards the jet flow is flat for ease of fabrication and installation of the backwall. An alternative of the flat backwall is a curved backwall which was experimentally proved in the FMIT project. It was demonstrated that, depending on the back-wall radius curvature, the jet stability may be improved [Hassberger 83]. An enlarged view of the beam-on-target region is shown in Figure 2.

The shape and dimension of the flow straightener, nozzle, backwall curvature, and downstream diffuser will be tested in laboratories using water initially, and lithium in subsequent mockup experiments.

A free jet target assembly has also been proposed. The main advantage of such an option is that it does not need the backwall replacement and, therefore, the target structure can be designed for a permanent lifetime. However, because there is no physical boundary between the target and the test assemblies, the test cell must be maintained at the same vacuum condition as the target chamber (10^{-3} Pa), which may be the limiting issue for this alternative.

2. THERMAL HYDRAULIC RESPONSE OF LI TARGET WITH INCIDENT DEUTERON BEAM

The CDA contribution of FZK for the IFMIF Target System has been started in 1995 by establishing a working environment for the evaluation of the thermal hydraulic response of the lithium target with incident deuteron beam.

Our study was concentrated on the analysis of lithium targets with parameters presented in Table 4, second column. The third column gives the nominal parameters recommended by the IFMIF CDA team in [IFMIF-CDA Final Report]. One should mention that our parameters set is appropriate for a deuteron beam of 35 MeV and it completely fulfills the recommended values for such a deuteron beam. The results we obtained for this configuration can easily be prolonged to other deuteron beam characteristics. In addition we like to emphasize that our studies are extended to all target configurations considered in the IFMIF-CDA, e.g. curved backwall (Curved BW), straight (flat) backwall (Flat BW) and free jet (FJ).

Table 4 *Lithium jet parameters*

	<i>250 mA @ 35 MeV D⁺</i>	<i>250 mA @ 40 MeV D⁺</i>
Jet thickness (m)	0.02	0.025
Jet width (m)	0.22	0.26
Jet velocity (m/s)	15÷22	15 (range 10÷20)
Inlet temperature (°C)	250	250
Outlet temperature (°C)	300	300 (for 15 m/s)
Surface temperature (°C)	290 (for 17.5 m/s)	290 (for 15m/s)
Peak temperature (°C)	390 (for 17.5 m/s)	400 (for 15 m/s)

2.1 MODELLING ASSUMPTIONS

In order to elaborate a computational fluid dynamics (CFD) model we started with the analysis of the beam-target physical processes.

The deuteron beam interacts with the flowing lithium in three different ways:

1. Kinetic energy transfer to the lithium through Coulomb ($\approx 98\%$) and nuclear processes; (energetic interaction).
2. Momentum transfer to the jet; (mechanical interaction).
3. Nuclear transmutation; (chemical interaction).

Scooping calculations were previously performed to assess the limit of response of the FMIT lithium target to the deuteron beam [Hassberger 83]. The main response modes investigated were the following: transient thermal response to the pulse nature of the deuteron beam, volumetric expansion effects and associated velocity field perturbation, surface tension gradients, momentum transfer induced

body force, sputtering due to direct collision events and chemical transmutation processes. Their results indicate that most response modes have acceptably minor impacts on the lithium target behavior.

We expect that the IFMIF target responses are much more tolerable due to an important reduction of more than an order of magnitude in the power deposition density (maximum power deposition density in IFMIF target is $\approx 150 \text{ kW/cm}^3$, compared with $\approx 1.8 \text{ MW/cm}^3$ in the FMIT target). This was confirmed by [Hassanein 96] which gives a detailed analysis of the jet thermal expansion and jet mechanical response for the IFMIF target.

The second step in assessing a CFD model is building a dimensionless group of the problem. That is summarized in Table 5 for the jet parameters reported in Table 4.

Table 5 *Dimensionless group of the problem*

Reynolds Number	$3.55 \cdot 10^5$	$Re = \frac{\rho UL}{\mu}$
Peclet Number	$1.73 \cdot 10^4$	$Pe = \frac{c_p \rho UL}{k}$
Froude Number	1560	$Fr = \frac{U^2}{gL}$
Weber Number	8030	$We = \frac{\rho U^2 L}{\sigma}$
Prandtl Number	0.049	$Pr = \frac{c_p \mu}{k}$
Turbulent Prandtl Number [Azer 60]	1.6	$P_t = \frac{1 + 380(Re Pr)^{-0.58}}{1 + 125 Re^{-0.45}}$
Capillary Number	0.022	$Ca = \frac{\mu U}{\sigma}$

where: U = main flow velocity, L = characteristic length, ρ = density, μ = dynamic viscosity, σ = surface tension, g = gravitational acceleration, k = thermal conductivity, c_p = heat capacity.

In conclusion, we have to solve a convection-dominated turbulent flow and heat transfer problem. In addition, the surface tension and gravitational effects seem to play no important roles. Due to the geometrical high aspect ratio, width over thickness of the jet, a two-dimensional model for a longitudinal cross-section throughout the flow could, in principle, account for an enough accurate description.

Preliminary calculations [Cherdron 96] have revealed that:

1. as the flow and heat transfer are convection dominated it is particularly important to provide an accurate simulation of the velocity distribution;
2. hence, it derives the significance of an accurate velocity profile at the nozzle exit;
3. whilst the laminar model gives acceptable solution for the core flow, only a turbulence approach can satisfactorily describe the global velocity and temperature field distributions, especially in the boundary regions.

Therefore we extended our studies to incorporate both the hydraulic analysis of the flow in the nozzle and the thermal hydraulic simulation of the lithium jet with free surface [Schütz 97].

2.2 MODELLING TOOLS

As main modelling tool we have used the finite element fluid dynamics analysis package FIDAP developed by Fluid Dynamics International, Inc., running on a Cray J90 computer. The energetics of the deuteron interaction in the lithium target was modeled within a special purpose computer program. Finally, a one-dimensional, Direct Simulation Monte Carlo (DSMC) program was used for the modelling of mass and heat transport in the IFMIF reaction chamber.

2.2.1 COMPUTING FLUID DYNAMICS MODELS

From the CFD models available in the FIDAP code we have selected:

- two-equations standard and extended k- ϵ turbulent models for the jet core momentum equations;
- the turbulent Prandtl number model for heat transfer in turbulent flows;
- the near-wall viscous sub-layer model for the momentum and energy equations.

TWO-EQUATION MODEL (k- ϵ)

In the k- ϵ model the turbulence field is characterized in terms of two variables, the turbulent energy k and the viscous dissipation rate of turbulent kinetic energy ϵ . Besides the Navier-Stokes equations system for momentum and energy conservation two additional transport equations for these two variables are solved.

An effective viscosity is calculated with the formula

$$\mu = \mu_0 + \mu_t \quad (1)$$

where μ_0 is the molecular viscosity and μ_t is the turbulent viscosity, expressed as:

$$\mu_t = C_\mu \rho_0 \frac{k^2}{\epsilon} \quad (2)$$

with $C_\mu=0.09$ and ρ_0 is the fluid density.

TURBULENT PRANDTL NUMBER METHODOLOGY

The laminar energy equation is solved for an effective thermal conductivity λ distribution prescribed by the relation

$$\lambda = \lambda_0 + \lambda_t \quad (3)$$

where: λ_0 is the molecular thermal conductivity and λ_t is the turbulent conductivity, expressed with the help of the turbulent viscosity μ_t and the turbulent Prandtl number P_t .

$$\lambda_t = \frac{c_p \mu_t}{P_t} \quad (4)$$

The determination of the turbulent Prandtl number is the main issue of this modeling methodology.

NEAR-WALL MODELING METHODOLOGY

In order to avoid a disproportionately large number of grid points for resolving sharply flow variables in regions adjacent to solid boundaries, one uses universal near-wall profiles to construct the shape functions for the special near-wall elements. Dimensionless velocity and temperature profiles become universal functions of y^+ , the characteristic non-dimensionalized distance from the wall

$$u^+ = f_u(y^+) \quad ; \quad T^+ = f_T(y^+, Pr) \quad ; \quad y^+ = \frac{\rho u_\tau \delta}{\mu} \quad (5)$$

where $u_\tau = (c_\mu)^{1/4} k^{1/2}$ is the friction velocity and δ is the normal distance from the wall.

The velocity profile is described as follows:

- linear velocity wall law in the viscous layer

$$u^+ = y^+ \quad ; \quad y^+ < 5 \quad (6)$$

- logarithmic velocity wall law in the fully turbulent region

$$u^+ = 1/K \cdot \ln(E y^+) \quad ; \quad y^+ > 30 \quad (7)$$

$K=0.41$ is the von Karman constant and E is a further empirical constant which equals 9.0.

In this methodology the k and ε equations are not solved in the special elements adjacent to the wall and the mixing length approach is adopted. Symmetry boundary conditions are applied for k and ε at the interface between the special elements and the fully turbulent region. In non-isothermal simulations it is recommended that the y^+ values be kept in the range $30 < y^+ < 300$.

It is worth to note that, in the case of heat transfer the transition from laminar to a fully turbulent state is also dependent on the laminar (molecular) Prandtl number. The applicability range of the universal wall profile law for heat transfer is from $P_t > 0.05$. Liquid metals are at the lower limit of this applicability domain (for example, liquid lithium at 250° has a molecular Prandtl number of $P_t = 0.05$).

2.2.2 POWER DEPOSITION MODEL

The profile of the deposited heat due to the stopping of the deuterons has been calculated for monoenergetic and Gaussian-shaped energy distribution of the beam. We used the stopping power data of reference [Andersen 77] which incorporates accurate models for both electronic and nuclear stopping powers (Table 6). According to this reference at low energies the stopping power is proportional to the projectile velocity and the high energy behavior is very well described by the Bethe formula. To bridge the gap between the high- and low-energy theories, interpolation formulas were proposed.

Table 6 Stopping power formulas

Energy (keV)	Stopping power (eV/10 ¹⁵ atoms/cm ²)
E=1 ÷ 10	$S=A_1 E^{1/2}$
E=10 ÷ 999	$S^{-1} = S_{\text{low}}^{-1} + S_{\text{high}}^{-1}$ $S_{\text{low}}=A_2 E^{0.45}$ $S_{\text{high}} = (A_3/E) \ln[1 + (A_4/E) + (A_5 E)]$
E=1000 ÷ 100,000	$S = \frac{A_6}{\beta^2} \left[\ln \left(\frac{A_7 \beta^2}{1 - \beta^2} \right) - \beta^2 - \sum_{i=0}^4 A_{i+8} (\ln E)^i \right]$

In the table above E is the deuteron energy per nucleon, $\beta^2=v_d^2/c^2$ where v_d and c are the deuteron and the light velocities, respectively. The values for the A_i coefficients are:

$A_1=1.411$	$A_2=1.6$	$A_3=725.6$	$A_4=3013$
$A_5=0.04578$	$A_6=0.00153$	$A_7=2.147 \cdot 10^4$	$A_8=-0.5831$
$A_9=0.562$	$A_{10}=-0.1183$	$A_{11}=0.009298$	$A_{12}=-0.0002498$

2.2.3 MASS AND HEAT TRANSPORT IN THE IFMIF REACTION CHAMBER

The main collisional quantities in a simple gas in the hard sphere approximation are expressed as follows:

Collision rate:

$$v_0 = 2^{1/2} \sigma_T n \bar{c} = (4/\pi^{1/2}) \sigma_T n (kT/m)^{1/2} \quad (8)$$

Equilibrium mean free path:

$$\lambda_0 = (2^{1/2} \sigma_T n)^{-1} = (2^{1/2} \pi d^2 n)^{-1} = \frac{16}{5} \left(\frac{m}{2\pi kT} \right)^{1/2} \frac{\mu}{\rho} \quad (9)$$

where: $\sigma_T=\pi d^2$ is the collision cross-section of a molecule with an effective diameter d , m is the molecular mass of the gas, n is the number density, T is the kinetic temperature, ρ is the mass density and μ is the viscosity coefficient.

Since the mean free path for the lithium target nominal conditions is $\lambda_0 \approx 8$ m, much higher than the enclosure typical size (≈ 1 m), we can apply the kinetic theory for collisionless flow. According to that, the mass transported by a flux of molecules which passes a unit of area is

$$m \cdot \Phi = \frac{1}{4} m \cdot n \cdot \sqrt{\frac{8kT}{\pi m}} = p_v(T) \sqrt{\frac{m}{2\pi kT}} \quad (10)$$

The energy flux from the liquid lithium surface reads

$$q_{Li} = mn\sqrt{\pi}(2RT)^{3/2} \quad (11)$$

where $p_v(T)$ and n are the saturated vapor pressure and concentration at temperature T .

As we have a temperature profile along the jet free surface, the mass and energy rates are dependent on the vertical position along the flow direction. The overall mass and energy rates are obtained by integration of the above relations over the free surface area with the temperature distribution on the free surface as delivered by FIDAP simulations.

One should note that for nominal pressures in the reaction chamber higher than 10^{-2} Pa or in case of accidental increase of the free surface temperature, the collisionless flow model is not valid and should be replaced, for example, by Monte Carlo Direct Simulation (DSMC). For this purpose we extended a one-dimensional DSMC program for non-condensable gas flow [Bird 94] to vaporization-condensation boundary conditions.

3. RESULTS AND DISCUSSION

As presented in the previous sections the full size problem involves: i) heat transfer in a turbulent flow, ii) presence of curved walls with different levels of curvature and, iii) presence of a free surface exposed to vacuum.

From the computational point of view, the simulation of the full size problem is prohibitively expensive. Therefore, besides the modeling assumptions listed in the section above, further simplifications were introduced by dividing the problem into three parts: 1) Hydraulic analysis of turbulent flow in the target nozzle; 2) Thermal hydraulic analysis of the lithium jet with incident deuteron beam and, 3) Assessment of the free surface effects on the jet flow. Figure 3 illustrates the philosophy of this approach. All parameters correspond to the reference target configuration.

3.1 HYDRAULIC ANALYSIS OF TURBULENT FLOW IN THE TARGET NOZZLE

A good nozzle design should provide a relatively uniform velocity profile at the outlet with a low turbulence and thin boundary layer. Our simulation of the flow through the target nozzle was not intended for the optimization of the nozzle design. To this purpose the recommended approach is to start with some empirically obtained design (for example, the asymmetric FMIT design which was also experimentally validated) and iteratively improve it both by water mock-up and numerical simulation. In our study we wanted to describe realistically enough the lithium flow in the target nozzle in order to investigate the influence of the jet inlet velocity and turbulence field profiles on the thermal hydraulic response of the lithium jet.

Without detailed information the FMIT design is difficult to reproduce rigorously. Hence, as target nozzle we assumed a 2-D symmetric Shima type reducer [JAERI-Conf 95, Kato et al.] which has the advantage of an analytical shape description (Figure 3a). The (transversal, longitudinal) coordinate pairs (x, y) are described by the relations:

$$\frac{x}{b} = \frac{1}{2\pi} \left\{ \left(\frac{a}{b} + 1 \right) \tanh^{-1}(\cos \theta) + \frac{1}{2} \left(\frac{a}{b} - 1 \right) \ln[2(1 - \cos 2\theta)] + \left[\sqrt{2 \left(\frac{a}{b} + 1 \right)} - \left(\frac{a}{b} + 1 \right) \right] \cos \theta \right\} \quad (12a)$$

$$\frac{y}{b} = \frac{1}{2} + \frac{1}{2\pi} \left\{ \left(\frac{a}{b} - 1 \right) \theta + \left[\sqrt{2 \left(\frac{a}{b} + 1 \right)} - \left(\frac{a}{b} + 1 \right) \right] \sin \theta \right\} \quad (12b)$$

where a and b are the width of inlet ($\theta=0$) and outlet ($\theta=\pi$), respectively.

Recent studies performed at the JAERI water loop test facility have demonstrated that a double-reducer nozzle of Shima type successfully provided a stable jet flow with a uniform velocity distribution [Nakamura et al. 97].

Thermal Hydraulic Response of Li Target with Incident Deuteron Beam

CFD Simulation:

- Finite element code FIDAP
- Turbulence model: k- ϵ
- Heat transfer model: turbulent Prandtl number

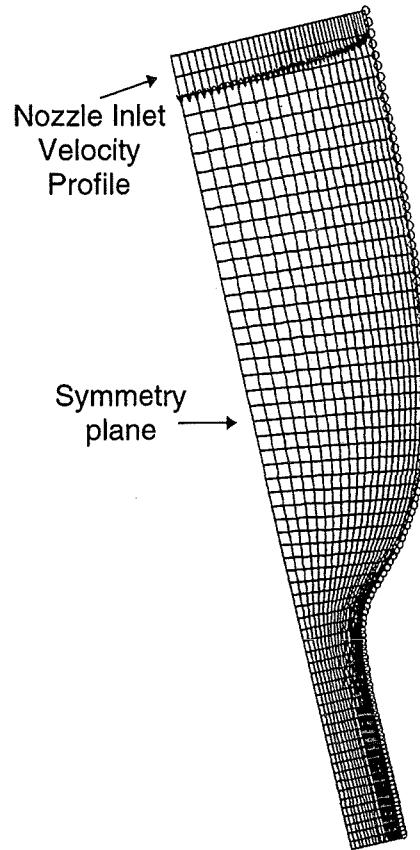
Configuration:

- Nozzle: 2-D Shima reducer model, contraction ratio ≈ 4
- Jet: Curved backwall target design, radius = 250 mm

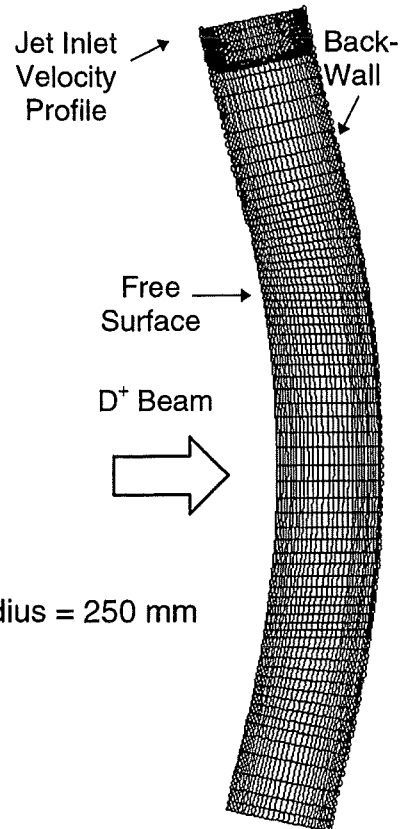
Heat Source Calculation:

Based on the heat deposition distribution of the following beam spatial profile

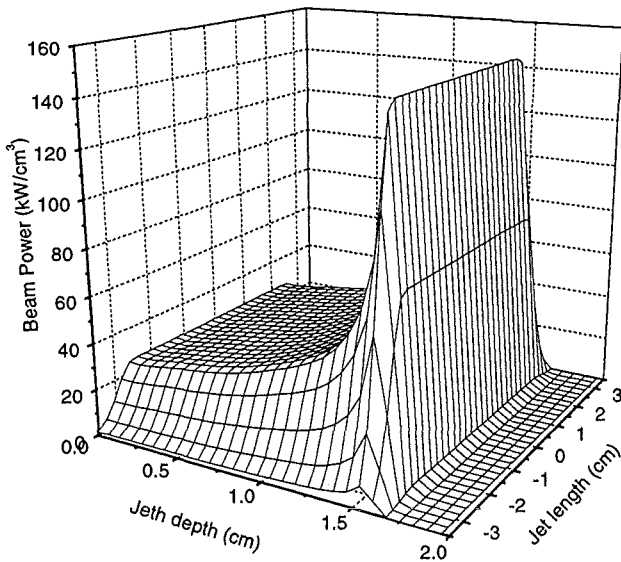
- Vertical direction: flat top of 5 cm; Gaussian edges of 1 cm
- Horizontal direction: flat with sharp edges
- Beam energy / current = 35 MeV / 250 mA
- Current density on flat top = 2.08 mA/cm²
- Average power deposition = 76 kW/cm²



a) Target Nozzle



c) Lithium Jet



b) Heat Source Profile

Figure 3. Set-up for the calculation of the thermal hydraulic response of a lithium target with incident deuteron beam (only right half of the symmetric nozzle shown).

As the nozzle inlet is preceded by a relatively long flow straightening section, the inlet boundary conditions could be modeled as fully developed channel flow:

Power law velocity profile:
$$u = u_{\max} \left(\frac{x}{\delta} \right)^{1/h} \quad (13a)$$

Turbulent kinetic energy:
$$k = c_{\mu}^{1/2} \left(l_m \frac{du}{dx} \right)^2 \quad (13b)$$

Dissipation:
$$\varepsilon = c_{\mu} k^2 \left(l_m^2 \left| \frac{du}{dx} \right| \right)^{-1} \quad (13c)$$

where x is the distance from the channel wall, δ is half of the channel width, h is a parameter dependent on the Reynolds number of the flow, and l_m is the mixing length, for example, as described by Nikuradse's formula:

$$l_m = \delta \left[0.14 - 0.08(1-x/\delta)^2 - 0.06(1-x/\delta)^4 \right] \quad (14)$$

With these boundary conditions, depicted in Figure 4 (left), the standard k - ε model produces the outlet profiles shown on the right of Figure 4. This result was obtained by solving the Navier-Stokes equations together with the k - ε transport equations for a nozzle with a contraction factor of about 4. The discretized model uses 1360 centered-quadrilateral elements with 9 nodes per element. The material properties correspond to the lithium inlet temperature of 250°C, see Appendix. Faster convergence to the stationary solution was obtained by employing an incremental Reynolds number strategy. The mesh size along the wall was tuned in order to achieve computed y^+ values (eq. 5) in the recommended range $30 < y^+ < 300$.

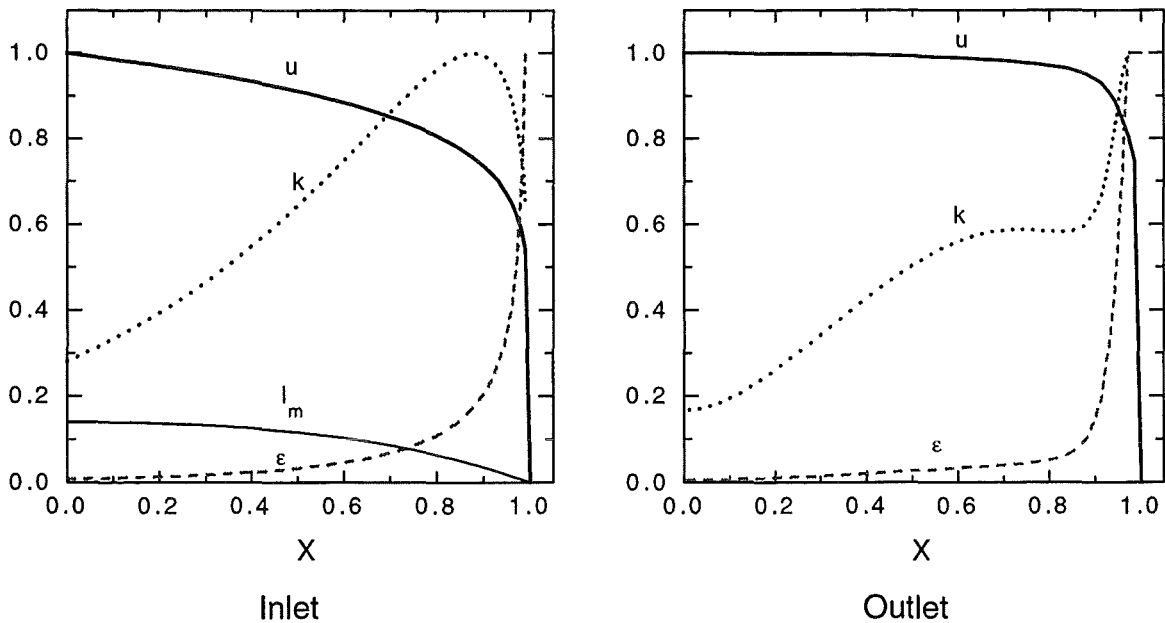


Figure 4. Inlet boundary conditions (left) and standard k - ε model outlet normalized profiles (right)

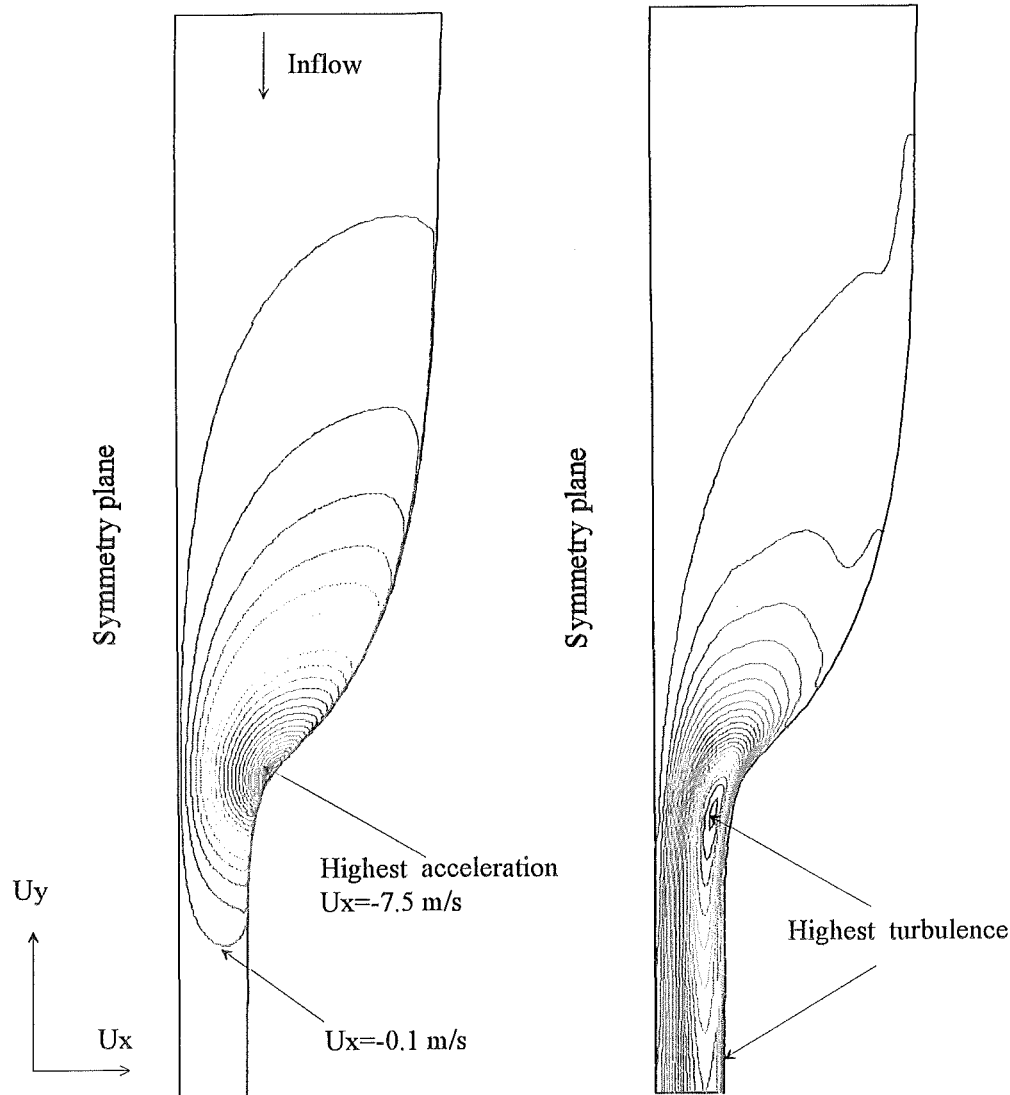


Figure 5. Contour maps of the x component of the velocity (left). On the right the contour maps of the turbulent kinetic energy is plotted. Inlet boundary conditions: fully developed flow with average velocity of 5 m/s.

The x component of the velocity at the nozzle outlet is an important parameter related to the mechanical stability of the jet. Figure 5 (left) gives the contour maps of the x component of the velocity at the nozzle outlet for an average inlet velocity of 5 m/s. Our simulation predicts a decay of the x component of the velocity from more than 7.5 m/s in the region with the strongest curvature to around 2 cm/s at the outlet plane on a flow path of about 3 channel widths.

On the right of the Figure 5 we show the contour maps of the turbulent kinetic energy for the same initial conditions. One can notice the correlation between the two pictures. The strong acceleration region displayed by the x component of the velocity seems to be the main source of turbulence. The transport of turbulent kinetic energy in both radial and axial directions is also clearly revealed. Obviously, the nozzle boundary layer acts as an additional source of turbulence.

One can remark that a relatively long nozzle generates a quasi-complete decay of the x component of the velocity, so improving the jet stability. In the same time a long nozzle generates a significant increase of the boundary layer with the associated instability caused by turbulence phenomena. A trade off value of the

nozzle length should be determined. For a round nozzle it has experimentally been found that long nozzles produce more unstable jets. Various methods are applied for the optimization of the IFMIF target nozzle [IFMIF-CDA Final Report 96].

In conclusion, a gradual change in the velocity and pressure profiles in the nozzle is preferable for a stable jet flow. Figure 6 gives velocity profiles at some streamwise positions together with the axial velocity and the reduced static pressure along the flow. The abrupt flow acceleration at the strongest curvature of the nozzle is associated with a steep increase in the reduced static pressure (total pressure divided by dynamic pressure). Measured back-wall static pressures for the FMIT target design had suggested that a relatively large curvature radius of the nozzle seems to be preferable for a smoother decrease in the pressure.

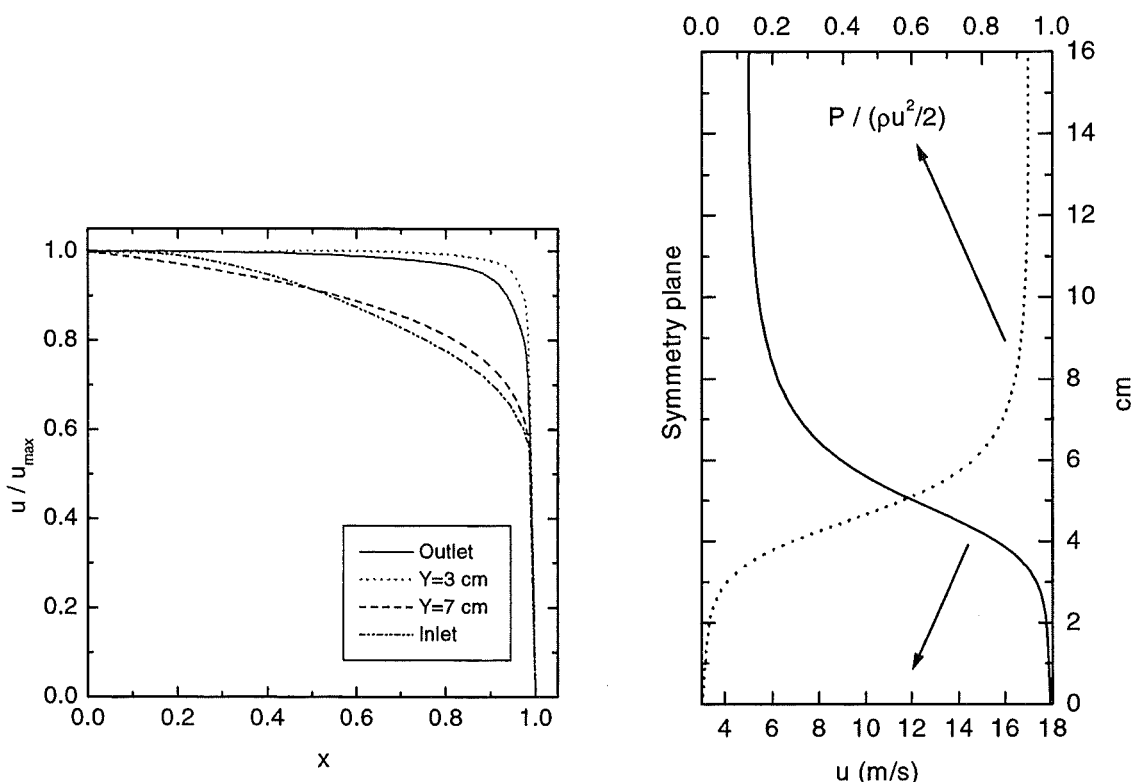


Figure 6. Velocity profiles at different streamwise positions (left). The y coordinate is measured from the outlet plane. Velocity and reduced static pressure axial profile (right).

We compared the results of the simulation of the liquid lithium flow through the Shima nozzle design for two Eddy Viscosity Models (EVM): the standard isotropic EVM and an anisotropic EVM due to [Speziale 87]. Speziale's model renders the Reynolds tensor a quadratic function of the strain rate tensor. It is claimed that this provides the necessary mechanism for predicting turbulent anisotropy effects [FIDAP User Manual]. The model has been shown to correctly account for the anisotropy of the turbulent normal stresses in boundary layer type flows and qualitatively predicts the weak secondary flows resulting from stress anisotropy in channels of non-circular cross-section.

As a result of this comparison, we noticed that the velocity and pressure fields are very similar for the range of the inlet average velocities studied. However, the turbulence fields are slightly different (Figure 7). While the distribution of the dissipation seems to be rather insensitive to the type of the EVM used, the

turbulent kinetic energy and, consequently, the turbulent viscosity distribution are similar as shapes but not as values.

It seems that the main difference is that the anisotropic model prediction is less diffusive in both the streamwise and spanwise directions. As consequence, the anisotropic EVM predicts higher turbulence at the outlet plane. Also the decay of the x component of the velocity along the flow direction is slightly slower predicted by the anisotropic model.

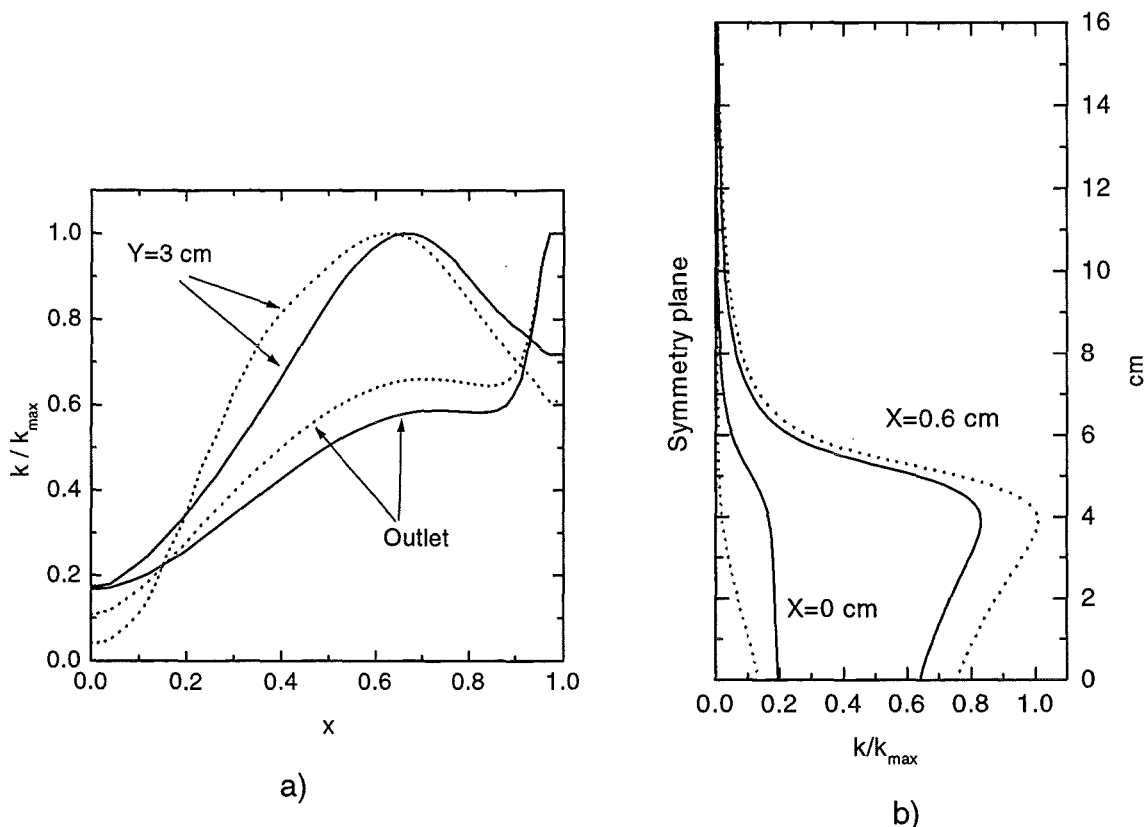


Figure 7. a) Turbulent kinetic energy at two stations; $k-\epsilon$ Boussinesq EVM (full line), $k-\epsilon$ Speziale EVM (dotted line). b) Axial distribution of the turbulent kinetic energy; $k-\epsilon$ Boussinesq EVM (full line), $k-\epsilon$ Speziale EVM (dotted line)

The results of the simulation with the isotropic standard $k-\epsilon$ model were retained as input data for the thermal-hydraulic analysis of the lithium jet. The main reason is that the anisotropic extension is a recent enhancement in the FIDAP code which should be further tested, especially for heat transfer problems.

3.2 THERMAL HYDRAULIC ANALYSIS OF THE LITHIUM JET WITH INCIDENT DEUTERON BEAM

The thermal response of the lithium jet is calculated by solving the heat conduction equation together with the turbulence hydrodynamics equations for the 2-D discretized jet.

An accurate description of the volumetric energy deposition rate of the incident deuteron beam is an essential ingredient for the solution of the heat conduction equation. To this purpose we applied the models presented in Table 6 for the calculation of the deuteron range and power deposition profile. These predict that

both the range and the stopping power are strongly dependent on the initial deuteron energy and energy distribution. While the deuteron penetration increases strongly with energy, the stopping power increases substantially with decreasing deuteron energy. One can also notice the dependence of the deuteron energy deposition distribution on the jet temperature profile. These trends are revealed in the Figure 8 where the power deposition profile for different deuteron energies and for different jet temperature profiles are represented.

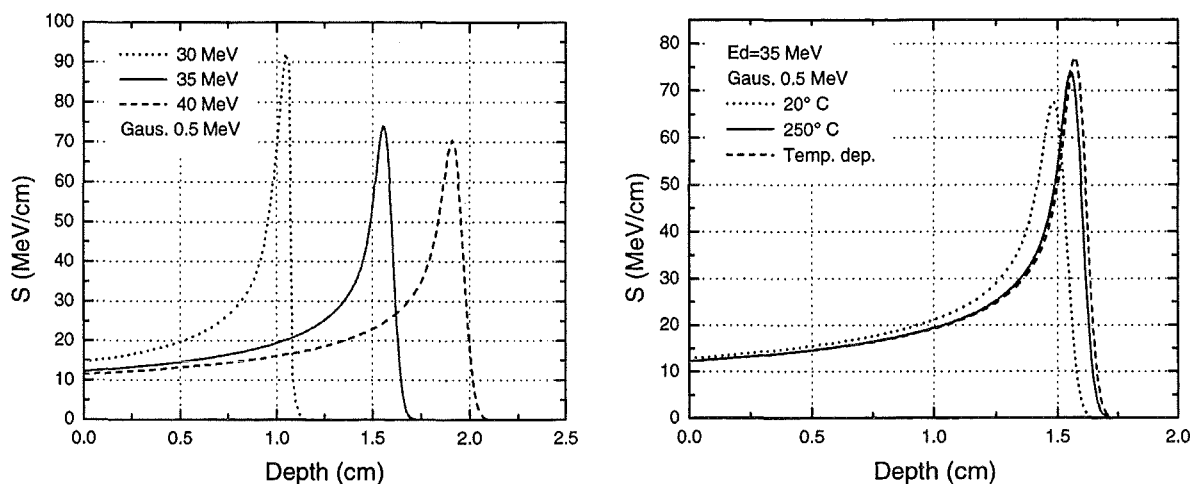


Figure 8. Deuteron energy deposition versus penetration depth for three incident energies (left). Deuteron energy deposition versus penetration depth for different jet temperature profiles (right). The broken line corresponds to the reference lithium jet temperature profile.

The Gaussian shaped energy distribution assumed in these calculations has two effects. Whilst slightly increasing the effective range, it is also responsible for a significant reduction in the Bragg's peak compared with that resulting from a monoenergetic distribution. The jet temperature profile influences the deuteron energy deposition through the temperature dependence of the lithium density. Higher average temperatures of the jet determine slight increases of the effective range simultaneously with the narrowing of the Bragg's peak. Obviously, this deuteron energy deposition profile will generate a similarly shaped temperature profile in the lithium jet. This could induce a kind of positive feedback of the Bragg's peak intensity with the local temperature. A possible solution would be the modulation of the deuteron energy with a wider Gaussian distribution. The results of this study also allow us to predict the optimum jet thickness in order to maximise the neutron flux at the test section, minimize the lithium flow rate, and ensure complete stopping of the incident beam. For a 35 MeV deuteron beam the optimum thickness is around 20 mm and it should be increased to up to 25 mm for 40 MeV average deuteron energy. At this point one can note that there are significant differences in literature both in the position of the Bragg's peak and the shape of the energy deposition profiles.

In order to obtain the volumetric heat source we have to modulate the power deposition profile with the superficial beam current distribution. The beam spatial profile in the vertical direction is shown in Figure 9. It is composed of two beams superimposed; the footprint of each is rectangular 7×20 cm². In the vertical direction the distribution is flat on a length of 50 mm with Gaussian edges of 10 mm. The average current density on the flat top is 2.08 mA/cm². In the horizontal

direction the distribution is flat with sharp edges. With these parameters it results a loading of 76 kW/cm^2 on the beam flat top.

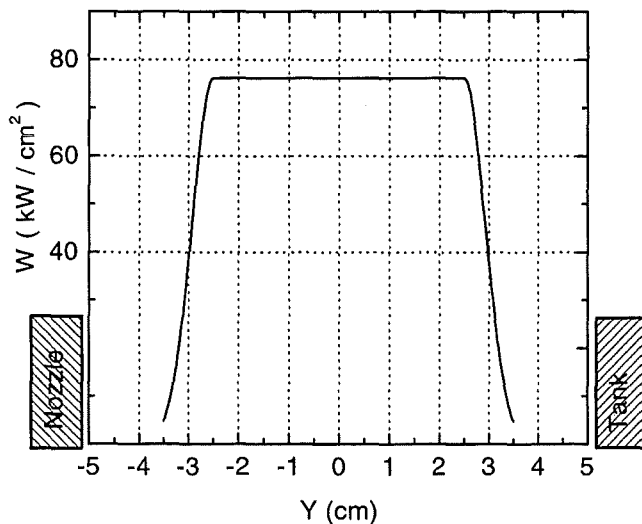


Figure 9. *Beam profile requirement: vertical direction*

For a 35 MeV deuteron beam Figure 10 gives the contour plot of a typical volumetric heat source distribution. One can divide the heated volume in three parts:

- a relatively uniform heating in the volume delimited by the jet free surface and the Bragg's peak region with a typical power density in the order of 25 kW/cm^3
- the Bragg's peak region with about 150 kW/cm^3 for the peak power density;
- the region between the Bragg's peak and the target back-wall with no direct deuteron beam energy deposition. The heat in this region is generated mainly by gamma rays and neutrons and it is expected to have very little contribution to the energetics of the jet. In our calculations the power density in this region takes assumed uniform values in the range of hundreds of W/cm^3 .

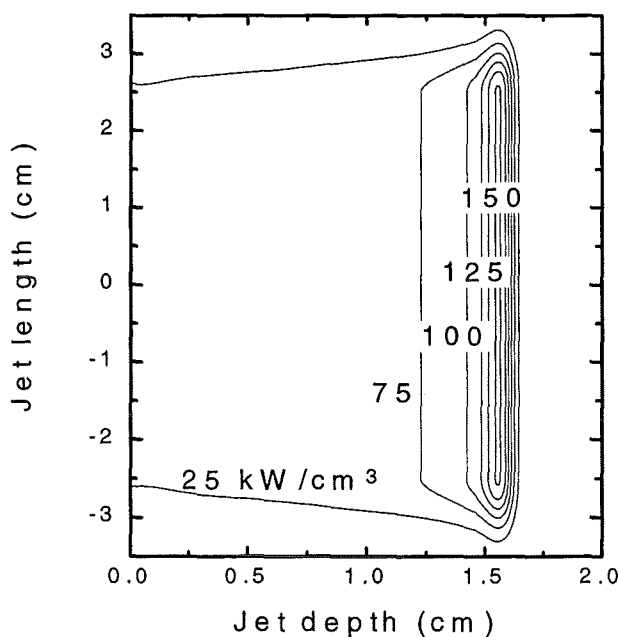


Figure 10. *Heat source profile ($E=35 \text{ MeV}$, $I=250 \text{ mA}$)*

Typical jet configurations start with an extension of the nozzle outlet of about two channel widths followed by the free jet and ended with another parallel channel of the same length (Figure 3c). The parallel channel extensions were introduced to ease the numerical control of the boundary conditions, especially for the pressure boundary conditions. The target jet was divided into 2444 of centered-quadrilateral elements with 9 nodes per element.

Temperature dependent material properties were used, see Appendix. Both the nozzle outlet velocity profile and the turbulence field were passed as inlet boundary conditions to the thermal hydraulic equation system. Faster convergence to the stationary solution was obtained by employing the incremental Reynolds number strategy. Again, the mesh size along the wall was tuned in order to achieve computed y^+ values (eq. 5) in the recommended range $30 < y^+ < 300$.

All three target concepts, e.g. curved back-wall, straight back-wall and free jet, have been simulated. In the following, we will present in more details the velocity, turbulence and temperature field distribution in the jet and the boiling margin and evaporation rate at the free surface as function of the nozzle initial boundary conditions and the turbulent Prandtl number.

The evolution of the velocity profile along the flow direction is given in Figure 11, both for the laminar and $k-\epsilon$ turbulence model. As expected, the flow in the core of the jet is similarly described by the two models. The main difference could be seen in the boundary layer velocity field; the turbulence model reproduces better the growing boundary layer and the free surface acceleration. These characteristics are essential in the description of the heat transfer at the boundary and especially at the free surface. Also notice that both models display a sloped velocity profile.

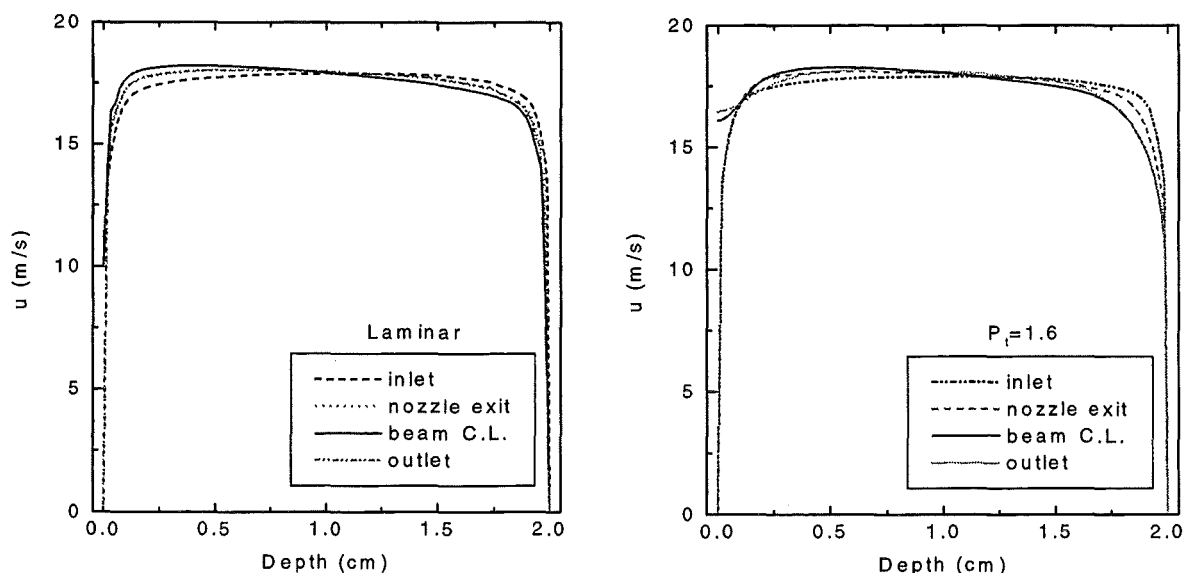


Figure 11. Evolution of the velocity profile along the flow direction. Laminar model calculation (left). Standard $k-\epsilon$ turbulent model calculation; $P_t=1.6$ (right).

Some typical characteristics of the turbulence field are illustrated in Figure 12 where the evolution of the turbulent kinetic energy and of the dissipation along the flow direction are represented.

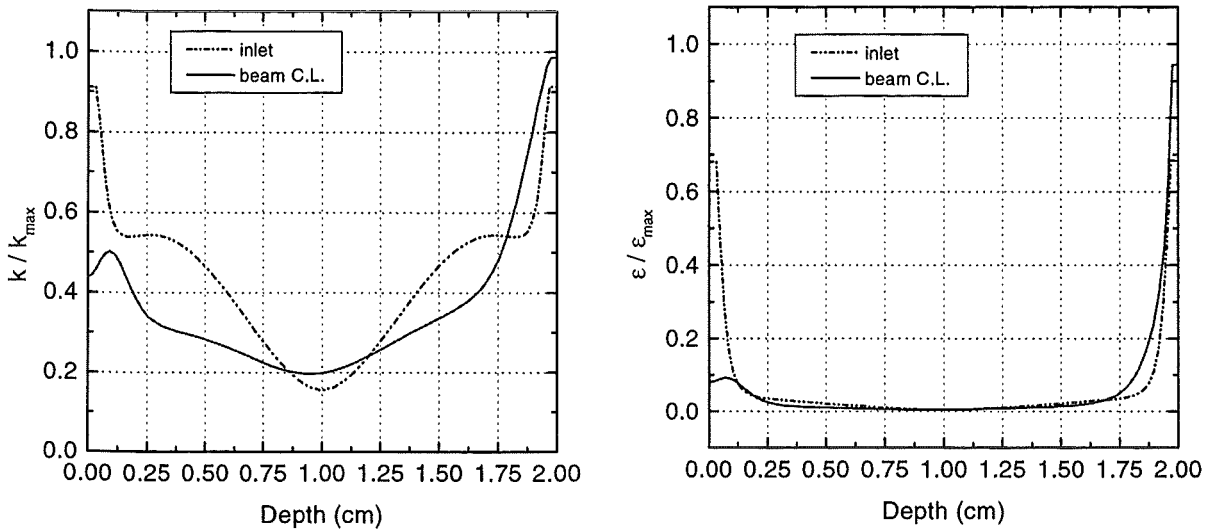


Figure 12. Evolution of the turbulent kinetic energy (left) and dissipation (right) along the flow direction. Standard k - ϵ model calculation; $P_r=1.6$.

One can remark the relatively fast decay of the turbulence along the free surface. However, this should be considered only as a qualitative result since the accuracy of turbulence models for flow with free surfaces is rather poor. The main reason in our case are the rather inadequate boundary conditions at the free surface for the transport equations of k and ϵ . The only recommendations available in FIDAP code are the symmetry boundary conditions which are known to overestimate the turbulence at the free surface [Rodi 80]. The same reference proposed a set of non-linear boundary conditions for better agreement with the experimental values for turbulence. The cost of this approach is an increased overall non-linearity of the problem with associated numerical difficulties.

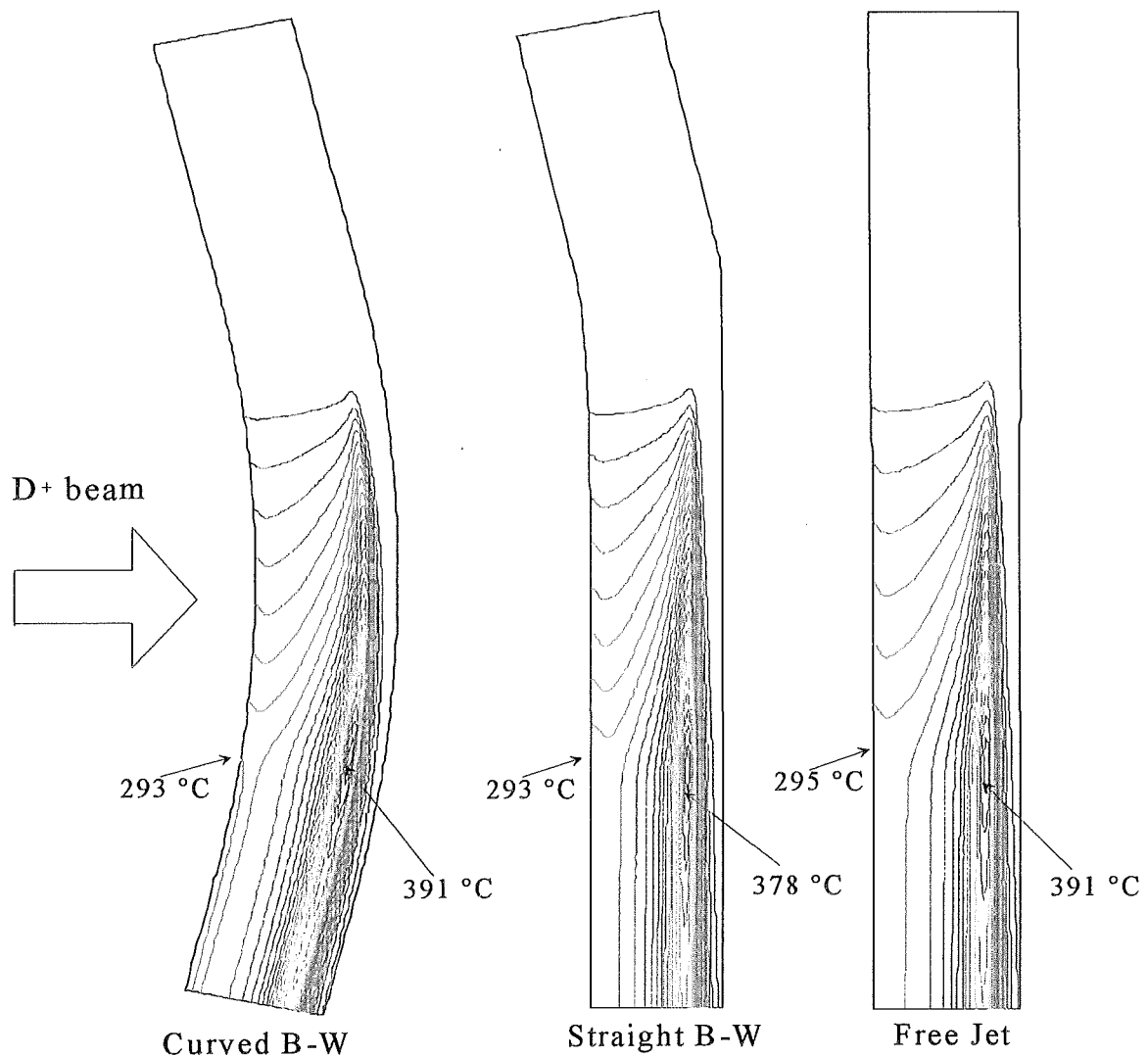


Figure 13. Temperature distribution contour maps for the three target concepts. Jet average velocity $U=17.4$ m/s, Inlet temperature $T=250$ °C. Maximum temperatures on the free surface and inside the jet are indicated.

Typical temperature distributions for all three target concepts are shown in Figure 13. One first observation is that the temperature profiles are practically not dependent on the target concept. As expected they retain the deuteron energy deposition pattern. The maximum temperature on the free surface is about 290 °C and is located at the lower edge of the beam footprint. The temperature peak inside the jet is roughly located at the same depth as the Bragg's peak and about 3 cm below the beam centerline. Some projections of the temperature map for the curved back-wall target concept are also illustrated in Figures 14 and 15.

As well known, determination of the turbulent Prandtl number is the main issue of this modelling methodology. A value of $P_t=1.6$ has been chosen in agreement with the global Reynolds number ($Re=3.5 \cdot 10^5$) for the liquid metal flows (see Table 5).

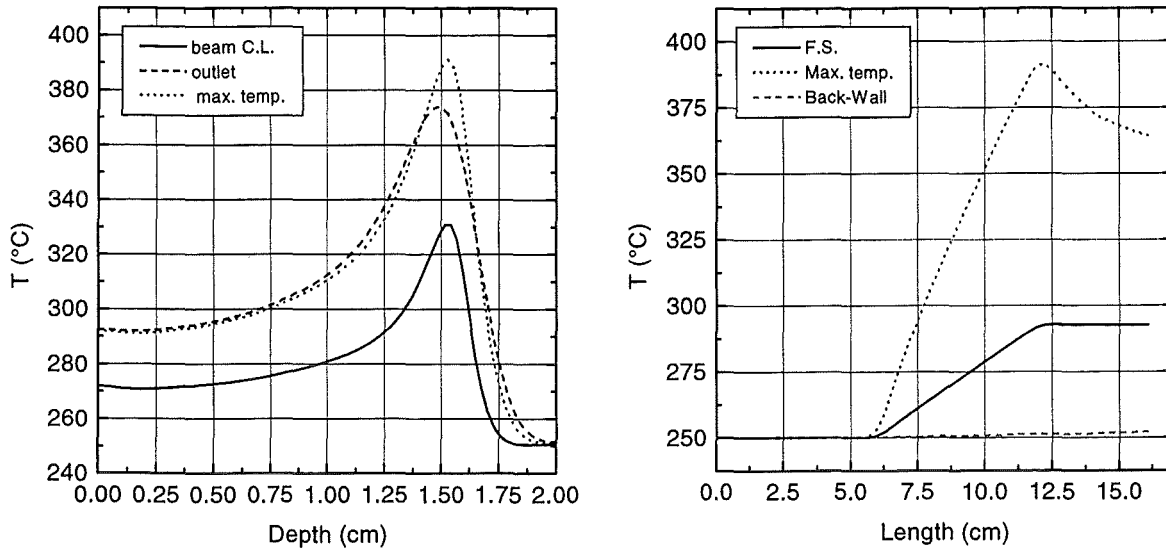


Figure 14. Temperature distribution at Beam Centerline C.L. (left). Evolution of temperature distribution in different cross-sections along the flow direction (right).

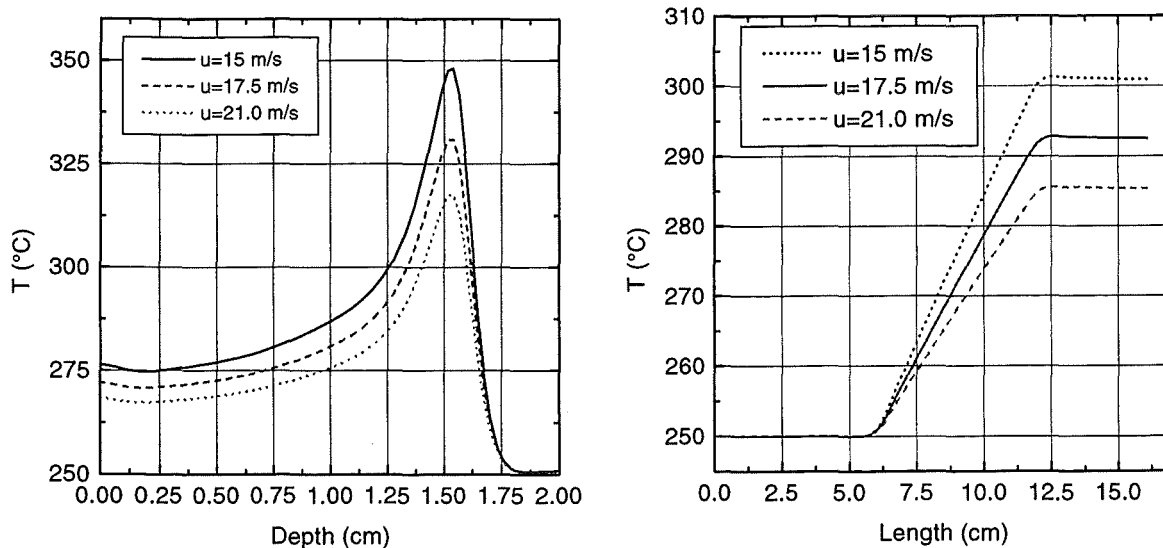


Figure 15. Temperature distribution at the beam C.L. (left) and at the free surface (right) for different jet inlet average velocities.

3.3 BOILING MARGIN AND EVAPORATION RATE

A series of representative results for different initial flow conditions and target configurations are given in Table 7. For the reference target concept with curved back-wall, three average velocities at jet inlet, respectively 14.6, 17.4 and 20.9 m/s corresponding to 4.2, 5.0 and 6.0 m/s at the nozzle inlet, are simulated. Then the reference case with an average jet inlet velocity of 17.4 m/s is analyzed for the straight back-wall and the free jet concepts.

The reported boiling margins values in the jet and at the free surface have been calculated using the local pressure distribution and the measured temperature dependence of the lithium saturation pressure (see Appendix).

Table 7 Laminar and standard $k-\epsilon$ turbulence model calculations for different flow initial conditions

		CURVED BW			STRAIGHT BW	FREE JET	
Input parameters		CASE A	CASE B	CASE C			
max. velocity at nozzle inlet (m/s)		4.2	5	6	5	5	
max. velocity at jet inlet (m/s)		15	17.9	21.5	17.9	17.9	
average velocity at jet inlet (m/s)		14.6	17.4	20.9	17.4	17.4	
inlet temperature (°C)		250	250	250	250	250	
Simulation results							
jet max temperature (°C)	Laminar	504.7	467	433			
	$P_t=1.6$	420.8	391.1	367.7	378.0	390.6	
FS max. temperature (°C)	Laminar	309.4	300	291.7			
	$P_t=1.6$	301.3	292.8	285.6	293.0	294.8	
max. pressure difference across the jet C.L. (Pa)	Laminar	9238	13147	18986		No internal pressure .	
	$P_t=1.6$	9110	12967	18733	497		
FS boiling margin (°C)	Laminar	33.6	43	51.3			
	• $T_b=343^\circ\text{C}$ at $p=10^{-3}$ Pa	$P_t=1.6$	41.7	50.2	57.4	50.0	48.2
	• $T_b=300^\circ\text{C}$ at $p=10^{-4}$ Pa	$P_t=1.6$	-1.3	7.2	14.4	7.0	5.2
evaporation rate $\times 10^{10}$ (Kg/s) $p=10^{-3}$ Pa	Laminar	6.89	4.38	2.96			
	$P_t=1.6$	4.58	3.04	2.15	3.04	3.07	

Note: The reference calculation results correspond to the case B ($U=17.4$ m/s , $P_t = 1.6$).

As expected, the laminar model predicts higher temperatures both in the jet and at the free surface (FS) and, consequently, a narrower boiling margin at the free surface. The reason is that the k- ϵ turbulence model predicts an effective viscosity of about two orders of magnitude higher than the molecular value, the corresponding turbulent thermal conductivity is up to one order of magnitude higher than the molecular value, with linearly dependence on the chosen P_t .

We studied the sensitivity of the main thermal characteristics of the lithium jet with incident deuteron beam to the Prandtl number for P_t values between 0.9 and 4.0. This allows us to assess the thermal response of the lithium jet both, at reduced and, especially, at enhanced heat transfer conditions. As results, we obtained that the maximum temperature at the free surface is practically not sensitive to the P_t while the maximum temperature inside the jet shows variations of about 15°C around the value calculated for $P_t=1.6$. To explain these results we should note, on one hand, that the temperature profile towards the jet free surface is rather flat (Figure 14). Hence, even important variations in the thermal conductivity will have a very reduced effect on the temperature profile in the free surface region. On the other hand, in the Bragg's peak region variations of the thermal conductivity properties should be accompanied by significant changes of the peak shape. However, in the flow conditions of interest the heat transfer by conduction is strongly dominated by the removal of the heat by convection and, hence, the changes in the peak temperature are rather moderate. These changes of the peak temperature are totally non-relevant for a target concept which preserves a significant level of the internal pressure. In conclusion, our results presented in Table 7 will stand even for special situations of instabilities driven enhanced heat transfer.

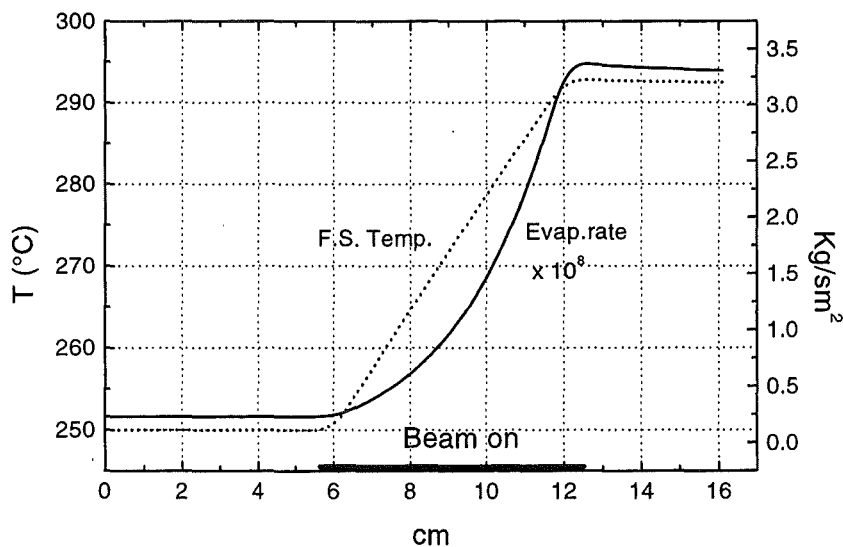


Figure 16. Temperature at the jet free surface and the evaporation rate calculated in the kinetic theory approach.

The evaporation rate was calculated in the kinetic theory approach, equation 10. An example which shows its strong non-linear dependence on temperature is given in Figure 16. The evaporation rate absolute values, generally within tolerable levels (few grams per year), should be taken as within a factor accurate due to the simplicity of the model and the scarcity of the saturation pressure data. At nominal reaction chamber pressures (10^{-3} - 10^{-4} Pa) employing a more realistic Monte Carlo direct simulation (DSMC) did not improve the accuracy since the main ingredients of the model are also rather poorly known. That is especially the case for the molecular radius and its temperature dependence for lithium and reaction chamber ambient gas. However, the DSMC is a preferable solution in case of nominal pressures in the reaction chamber higher than 10^{-2} Pa or in case of accidental increase of the free surface temperature when the collisionless flow model is not longer valid.

At an average jet speed of 17.4 m/s all three target concepts provide a relatively safe boiling margin at the free surface. For a pressure in the reaction chamber of $p=10^{-3}$ Pa which corresponds to a lithium boiling point $T_b=343$ °C, the boiling margin at the free surface is about 50 °C; at $p=10^{-4}$ Pa with $T_b=300$ °C, the boiling margin is reduced to only 7 °C.

In case of the curved back-wall concept, due to the centrifugal force inside the jet the pressure increases quasi-linearly from the reaction chamber pressure until $p\approx 1.3\cdot 10^4$ Pa near the back-wall such that boiling inside the jet is strongly prevented. As can be seen in Figure 17, the boiling margin in this case exceeds several hundreds of Celsius degree. For the boiling margin evaluation we took into account the temperature profile in a jet cross-section passing through the temperature peak located about 3 cm below the beam centerline.

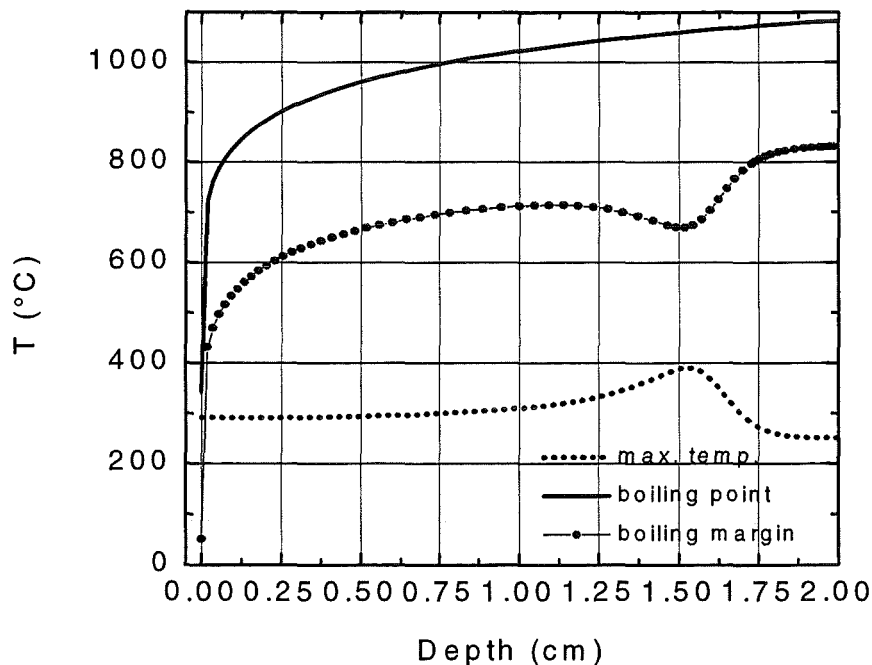


Figure 17. Distribution of the boiling point and boiling margin; reference target concept, (Curved B-W, $p=10^{-3}$ Pa).

The straight back-wall target configuration due to a reduced and fast decaying internal pressure along the flow provides only a limited boiling margin inside the jet, up to several tens of degree at a station a few cm below the beam centerline. As can be seen in Figure 18, the pressure along the flow through the maximum temperature cross-section is reaching values in the range of several tens of Pa just a few centimeters below the beam center line.

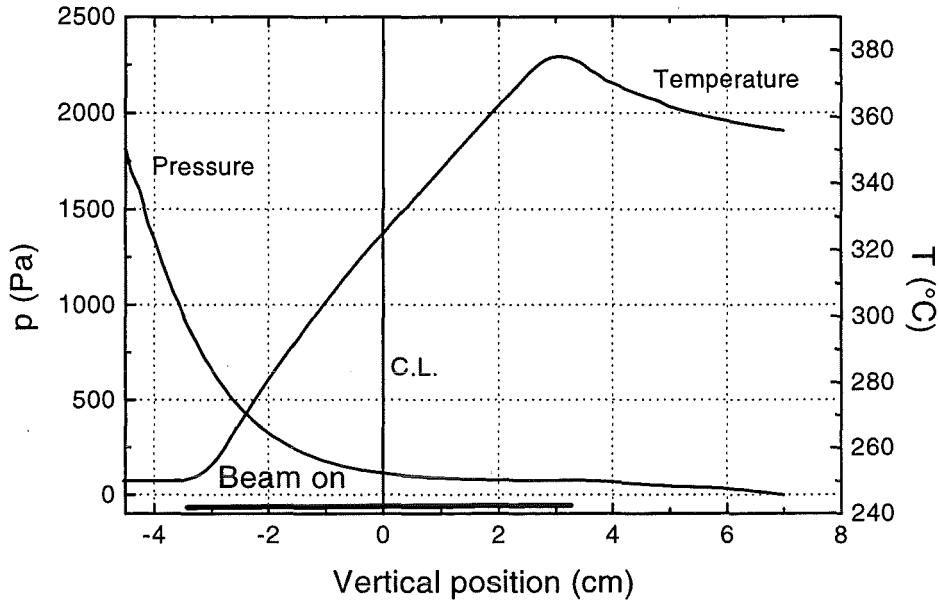


Figure 18. Pressure distribution along the flow through the maximum temperature cross-section. (Straight B-W target concept)

On the other hand, the lack of internal pressure of the free jet concept necessitates a significantly increased jet average speed in order to avoid extensive contamination of the accelerator vacuum by nucleate boiling of the jet.

Concerning the free surface effect on the jet flow our simulation has shown a very small reduction in the thickness of the lithium jet for the curved back-wall and the free jet target concepts. However, for the straight back-wall concept our calculations revealed a significant shrinking of the jet with up to 10% (≈ 2 mm) of the inlet jet thickness which affects the jet temperature distribution. Obviously, the shrinking effect is associated with the flow acceleration and, consequently, a slight reduction in the peak temperature inside the jet. In order to compensate for the shrinking tendency, the initial thickness of the jet should be correspondingly increased.

This image could be completed with the following comparison between the three target concepts (Table 8).

Table 8 *Comparison between target concepts*

CURVED BW	<ul style="list-style-type: none">• experimentally proved feasibility (FMIT project, USA)• good stability of jet free surface• presence of centrifugal internal pressure prevents nucleate boiling• minimum lithium inventory of the three concepts
STRAIGHT BW	<ul style="list-style-type: none">• relatively simple manufacturing and remote control replacement• our calculations revealed a significant shrinking of the jet with up to 10% (≈ 2 mm) of the inlet jet thickness which affects the jet temperature distribution• jet free surface stability: not yet tested• jet internal pressure is fast decaying along the flow; consequently, the nucleate boiling could be a limiting issue for this target design• increased lithium inventory for acceptable performances of the target
FREE JET	<ul style="list-style-type: none">• no need for backwall replacement• jet free surface stability: not yet tested• no internal pressure; consequently, the nucleate boiling could be a limiting issue for this target design• very high lithium inventory for acceptable performances of the target

3.4 COMPARISON WITH OTHER WORKS

This section will be devoted to a comparative discussion of similar studies for the thermal hydraulic analysis of a lithium jet with deuteron beam published in the open literature so far. These include the original works performed in the FMIT project [Hassberger 81, 83] and more recently, communications or articles issued in the frame of the IFMIF project: Kato, Y. et al., Hua, T and Cevolani, S. in [JAERI-Conf 95], [Hassanein 96] and [Nakamura et al. 97]. In general, these studies refer to the curved back-wall target concept. The Hassanein's results are obtained by solving a time-dependent heat conduction equation which, in principle, ignores the detailed jet velocity profile.

A first aspect to be discussed is the ability of the employed models to describe the velocity and temperature field of the jet. For that reason we compared the reported results with an analytical asymptotic velocity distribution. A simple description of the one-dimensional curved jet flow could be based on the assumption of fully developed potential flow. For a surface velocity v_0 and a surface radius of r_s , the asymptotic irrotational velocity distribution with the radius r is:

$$v = v_0 \frac{r_s}{r} \quad (15)$$

A comparison between measurements and prediction of the velocity distribution in the Plastic Model Water Tests, conducted within the FMIT project, shows that the potential flow solution accurately describes the shape of the velocity profile within the limits of the omitted boundary layers. Very recently, [Nakamura et al. 97] in experiments performed at the JAERI water loop test facility, which uses a double-reducer of Shima type, have also demonstrated a good agreement with the velocity profile expressed in equation (15).

Figure 19 gives the shape of this velocity distribution together with our results for the velocity profile at beam centerline. One can note that the analytical distribution is well reproduced in the jet core. Naturally, the 2-D simulation also provided the boundary layer velocity profile.

In general, the quoted references for the thermal analysis of the lithium jet with deuteron beam failed to reproduce the sloped pattern of the analytical result despite of the use of different CFD codes. Only in the reference Kato, Y. et al. in [JAERI-Conf 95] we found an apparently correct slope of the velocity profile. Actually in this reference we found also a consistent simulation of the lithium flow in both the target nozzle and the jet itself.

Concerning the free surface effect on the jet flow our simulation has shown a very little reduction in the thickness of the lithium jet for the curved back-wall and the free jet target concepts. This behaviour was also predicted in the simulation of Cevolani, S. in [JAERI-Conf 95] and experimentally proved in the FMIT project and, quite recently, at JAERI water loop facility. However, for the straight back-wall concept our calculations revealed a significant shrinking of the jet with up to 10% (≈ 2 mm) of the inlet jet thickness which affects the jet temperature distribution.

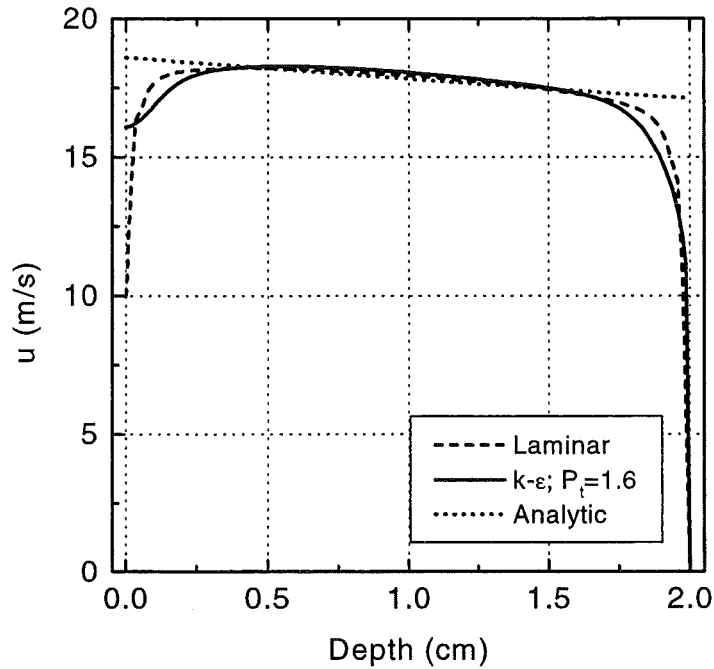


Figure 19. Velocity profile at beam centerline; laminar, standard $k-\epsilon$ model and asymptotic irrotational calculations.

The main parameters of interest for the temperature field are the maximum temperatures as well as their positions on the free surface and inside the lithium jet. In general, for the same flow conditions, such parameters have differences in the range of 10°C for temperature peaks and around 1 mm in the jet depth and couple of millimeters along the flow. As we noticed above the energy deposition profile of the deuterons is an essential ingredient in the heat transfer calculation and could be responsible for the main part of such variations in the jet temperature field. Different velocity profiles assumed or simulated could also explain the noticed differences in the free surface temperature distributions. Nevertheless, even including these differences, the overall set of calculations still confirms the physical feasibility of the IFMIF target in the curved back-wall configuration.

4. CONCLUSIONS

An analysis of deuteron energy deposition and thermal hydraulic response of the liquid lithium target has successfully been performed with the FIDAP code. To our knowledge this is one of the very few studies which includes a consistent simulation of the turbulent flow in both the target nozzle and the jet itself with application to all major target configurations.

Although we used a different fluid-flow simulation code and a different lithium properties data set, most of our results for the reference IFMIF target are consistent with those of the IFMIF partner groups. Thus, the surface vaporisation proved to be relatively small for the beam and jet parameters studied. The free surface at the lower edge of the deuteron beam has been identified as the most critical area for boiling. For relatively low pressures in the vacuum chamber (lower than $p=10^{-3}$ Pa) one can note that the boiling margin at the free surface (for example $\Delta T_b \approx 7$ °C for $p=10^{-4}$ Pa) is the limiting issue of the lithium target design.

The boiling margin inside the jet seems to be strongly sensitive to the target concepts. In case of the curved backwall concept, due to the centrifugal force inside the jet the pressure increases quasi-linearly from the reaction chamber pressure until $p \approx 1.3 \cdot 10^4$ Pa near the back-wall such that boiling inside the jet is strongly prevented. For other concepts like the straight back-wall which allows limited internal pressure inside the jet or like the free jet target which allows no internal pressure, boiling can be prevented only with the price of a significant increase of average jet velocity and consequently increased lithium inventory. In addition, previous investigations in the frame of the FMIT project and very recently at the JAERI water loop test facility have demonstrated the hydraulic stability of the curved back-wall target concept. In conclusion, it seems that the curved back-wall target concept should be preferred in the initial phase of operation.

The impact of the amount of vaporized lithium, its deposition and its interaction with the incident deuteron beam need further analysis. In this respect we proposed the use of a Monte Carlo Direct Simulation code for modeling of mass and heat transport in the lithium target reaction chamber and in the target-accelerator interface.

We can conclude that the results obtained in this study corroborated with other investigations have confirmed the physical feasibility of the IFMIF target in the reference curved back-wall configuration.

The models and methodology developed in this study could be used, with adequate modifications, for the investigation of other liquid metallic targets exposed to intense energy beam like: tokamak divertor cooled with liquid lithium, spallation target for intense neutron sources, fusion reactor liquid blankets, etc.

This work has been done within the frame of the EURATOM - FZK association.

REFERENCES

- [**Anderson 77**] Anderson, H.H. and Ziegler, J.F., *Hydrogen Stopping Powers and Ranges in All Elements*, Vol. 3, Pergamon Press (1977)
- [**Azer 60**] Azer, N.Z. and Chao, B.T., *A mechanism of turbulent heat transfer in liquid metals*, Int. J. Heat Transfer, Vol. 1, pp.121-138, (1960)
- [**Bird 94**] Bird, G.A., *Molecular gas dynamics and the direct simulation of gas flows*, Oxford Press, Oxford (1994)
- [**Cherdron 96**] Cherdron, W., Schütz, W. and Tiseanu, I., *Thermal hydraulic analysis of IFMIF target with incident deuteron beam*, Proc. of Jahrestagung Kerntechnik '96, Mannheim 21-23 Mai 1996, pp.609 - 612
- [**Ehrlich 95**] Ehrlich, K., Lindau, R., Proc. of the IEA technical workshop for an Intern. Fusion Materials Irradiation Facility, FZKA Report 5553 (1995)
- [**Ehrlich 97**] Ehrlich, K., Möslang, A., *International Fusion Materials Irradiation Facility (IFMIF): User Requirements and Test Cell Design*, Proc. of Jahrestagung Kerntechnik '97, Aachen 13-15 Mai 1997, pp.550 - 553
- [**FIDAP Users Manual**] Fluid Dynamics Analysis Package, FIDAP Users Manual, Revision 7.0-7.61, 1993-96
- [**Hassanein 96**] Hassanein, A., *Deuteron beam interaction with lithium jet in a neutron source test facility*, J. Nucl. Materials **223-237**, pp.1547-1551 (1996)
- [**Hassberger 81**] Hassberger, J.A., *Velocity distributions in the FMIF liquid lithium target*, HEDL-TME 81-32 (Handford Engineering Development Laboratory, Richland, WA, September 1981)
- [**Hassberger 83**] Hassberger, J.A., *Preliminary assessment of interactions between the FMIF deuteron beam and liquid lithium target*, HEDL-TME 82-28 (Handford Engineering Development Laboratory, Richland, WA, March 1983)
- [**IFMIF-CDA Final Report**] International Fusion Materials Irradiation Facility Conceptual Design Activity, Final Report, IFMIF Team, edited by M. Martone, ENEA Frascati Report, RT/ERG/FUS/96/11, December (1996)
- [**JAERI-Conf 95**] IFMIF-CDA Technical Workshop on Lithium Target System, JAERI-Conf 95-019, July 18-21, 1995, JAERI, Tokai, Japan
- [**Nakamura 97**] Nakamura, H., Itoh, K. and Kukita, Y., *Water Experiment of High-Speed, Free-Surface, Plane Jet Along Concave Wall*, submitted to NURETH-8 (8th International Topical Meeting on Nuclear Reactor Thermal-Hydraulics, to be held at Kyoto on Sept. 30 to Oct. 4, (1997)
- [**ORNL/M-4908**] International Fusion Materials Irradiation Facility Conceptual Design Activity, Interim Report ORNL/M-4908, compiled by M.J.Rennich, Oak Ridge, USA, December 1995

[Rodi 80] Rodi,W., *Turbulence models and their application in hydraulics - A state of the art review*, IAHR - Publication, Delft, (1980)

[Schütz 97] Schütz,W. and Tiseanu,I., *Thermal hydraulic analysis of IFMIF target including free surface and nozzle*, Proc. of Jahrestagung Kerntechnik '97, Aachen 13-15 Mai 1997, pp.554 - 557, (1997)

[Speziale 87] Speziale,C.G., *On Nonlinear k-l and k-ε Models of Turbulence*, Journal of Fluid Mechanics, 178, pp.459-475, (1987)

APPENDIX

Review of Lithium Physical and Thermal Properties

Main References

1. R.W. Ohse, Editor, Handbook of Thermodynamic and Transport Properties of Alkali Metals, Blackwell Scientific Publications (1985)
2. Handford Engineering Development Laboratory, HEDL-TME 78-15 (1978)

Properties Reviewed

Liquid lithium

Density
Viscosity
Specific Heat
Thermal Expansion Coefficient
Thermal Conductivity
Liquid Surface Tension

Lithium Vapours

Vapour Pressure
Viscosity
Thermal conductivity

Density of Lithium

ρ [Kg m ⁻³]	Temperature Range
$\rho = 508.2 - 0.10336(t - 271.7) - 4.8279 \cdot 10^{-7}(t - 271.7)^2 - 5.2853 \cdot 10^{-9}(t - 271.7)^3$	300 - 1000 °C
$\rho = 515 - 0.101(t - 200)$	200 - 1600 °C
$\rho = 536.8 - .103t$	400 - 1125 °C
$\rho = \sum_{i=0}^6 a_i (T/1000)^i$	460 - 3620 K
$a_0 = 0.53799943E+00$	$a_1 = -0.16043986E-01$
$a_2 = -0.99963362E-01$	$a_3 = 0.54609894E-01$
$a_4 = -0.15087628E-01$	$a_5 = 0.27045593E-02$
$a_6 = -0.31537739E-3$	

Note: T (K) = t (°C)+273.15 ; this relation applies everywhere in this Appendix.

Viscosity

μ [Pa s]	Temperature Range
$\ln \mu = -4.16435 - 0.6374 \ln T + \frac{292.131}{T}$ (Pa s)	460 - 3000 K
$\log \mu = -1.5064 - 0.737 \log T + \frac{109.9}{T}$ (Pa s)	200 - 1000 °C
$\log \mu = -4.338 + \frac{726.1}{T}$ (Pa s)	600 - 1200 °C

Specific Heat

c_p [J Kg ⁻¹ K ⁻¹]	Temperature Range
$c_p = 4530.2 - 0.838t$	181 - 420 °C
$c_p = 4207.6 - 0.0733t$	420 - 900 °C

Thermal conductivity

k [W m ⁻¹ K ⁻¹]	Temperature Range
$k = 42.29 - 0.0123t$	250 - 950 °C
$k = 34.50 - 0.0312t$	320 - 850 °C
$k = 45.6 - 8.29 \cdot 10^{-3}t$	300 - 900 °C
$k = 43.88 + 0.0209(t - 180.6) - 2.43 \cdot 10^{-6}(t - 180.6)^2$	300 - 1100 °C

Surface Tension of Lithium

σ_s [N/m]	Temperature Range
$\sigma_s = 1.6 \cdot 10^{-4}(3550 - T) - 9.5 \cdot 10^{-2}$ (T in K)	500 - 1600 °C
$\sigma_s = \frac{3.53 \cdot 10^6}{\rho^2} \exp\left(-\frac{1815}{T}\right)$	200 - 1300 °C ρ is density in Kg/m ³

Vapour Pressure of Lithium

P [Pa]	Temperature Range
$\log P = 19.218 - \frac{8551.2}{T} - 3.80 \log T + 6.72 \cdot 10^{-3}T - 6.4 \cdot 10^{-6}T^2 + 2.684 \cdot 10^{-9}T^3$ (T in K)	0 - 181 °C
$\log P = 15.124 - \frac{8442.5}{T} - 1.640 \log T + 2.597 \cdot 10^{-4}T$	181 - 1077 °C
$\log P = 12.404 - \frac{8283.1}{T} - 0.7081 \log T$	800 - 1400 °C